JOURNAL OF GEOPHYSICAL RESEARCH, VOL. 111, C03009, doi:10.1029/2005JC003030, 2006

Gravity waves interacting with a narrow jet-like current

R. D. MacIver,[1] R. R. Simons,[1] and G. P. Thomas[2]

Received 28 April 2005; revised 28 September 2005; accepted 18 November 2005; published 21 March 2006.

[1] A unique experiment to investigate the transformation of near-linear gravity waves propagating across a narrow horizontally sheared jet-like current, typical of those found in the nearshore, coastal, and ocean regions, is described. A single wave condition was studied, propagating across the current orthogonally and at oblique incidence in both a following and opposing sense to the current. The length scale of the current shear layers was comparable to the incident wavelength. The experiment is the first attempt to assess the kinematics and dynamics of the interaction of regular waves and currents in three dimensions at a physically realistic scale. The resulting data set provides direct quantitative measurements of the spatial variation of the primary flow variables. Negligible reflection of the incident wave at the current shear layers was observed. Typical refraction behavior was observed: A following wave is refracted to a more current-parallel direction with an increased wavelength and reduced wave height as it moves onto the current, while the opposing wave becomes more current normal with a shortened wavelength and enhanced wave height. The experimental data are compared with predictions of a wave ray model, assuming a depth-averaged current and slowly varying horizontal shear, and a new model that incorporates the influence of vertical shear.

Citation: MacIver, R. D., R. R. Simons, and G. P. Thomas (2006), Gravity waves interacting with a narrow jet-like current, *J. Geophys. Res.*, *111*, C03009, doi:10.1029/2005JC003030.

1. Introduction

[2] Waves moving across spatially varying mean flows may experience significant changes in amplitude, phase speed, direction, kinematics and bed friction, all of which affect both their local characteristics and their potential impact on the environment. Despite a widespread qualitative understanding, [*Jonsson*, 1990] provides the example of Polynesian sailors identifying the location of currents by observing the transformation of surface waves, a quantitative understanding remains incomplete. This is not for lack of attention. Wave-current interaction has been studied widely, with developments in the subject being reviewed regularly; major reviews have been conducted by *Peregrine* [1976], *Jonsson* [1990], and *Thomas and Klopman* [1997]. However, an enduring conclusion has been that contemporary knowledge has significant shortcomings and the subject requires further study.

[3] Accurate modeling of the morphodynamics of the nearshore environment, in which waves play a dominant part, relies fundamentally on the correct modeling of wave transformations to allow the nearshore wave field to be determined from the offshore incident wave conditions. One of several key aspects identified by *Hamm et al.* [1993] as being necessary for the correct prediction of the nearshore wave field was wave refraction by horizontally sheared currents such as those formed at river mouths, tidal inlets, tidal races and around coastal structures where the shear layers are typically of the same length scale as the incident wave. Recent measurements of increased directional spread in the surf zone have been associated with shear waves, streamwise variations of the transverse velocity of longshore currents (S. M. Henderson et al., Refraction of surface gravity waves shear waves, submitted to *Journal of Physical Oceanography*, 2005).

[4] Modeling of the interaction between regular waves and horizontally sheared currents can be classified on the basis of the width and rate of change of the horizontal shear layers of the current. Slowly varying models assume broad shear layers with relatively slow variations in current properties, allowing ray tracing and conservation of wave action to be used (see the comprehensive reviews of *Peregrine* [1976] and *Jonsson* [1990]). Classic ray theory assumes no vertical variation in the current profile, although the derivation by *White* [1999] imposes no such assumptions. Ray theory fails in the presence of a caustic where reflections can be expected. An application to a jet-like current by *McKee* [1977] found that two such caustics can exist, one associated with each of the positive and negative gradients of the shear layer. The asymptotic analysis, developed in earlier papers of a more general nature, determined a formula for the reflected wave and considered the trapping of waves on the current. The Mild Shear model of *McKee* [1987, 1996] permitted some weakening of the condition that the current changes extremely slowly. The approximation is equivalent to the mild-slope theory of *Kirby* [1984] for the case of constant water depth and the

[1]Department of Civil and Environmental Engineering, University College London, London, UK.
[2]Department of Applied Mathematics, University College Cork, Cork, Ireland.

0148-0227/06/2005JC003030$09.00

current shear is the result of external forcing with the requirement that the ratio of wavelength to shear layer thickness is small, in some sense. It is of note that reflected wave solutions are permitted.

[5] While a slowly varying approach is suitable for large-scale oceanographic applications it is less appropriate for many wave-current interactions in the nearshore region, where the current changes may occur over relatively short scales and both horizontal and vertical shear may be important. Vortex sheet models assume the shear layers of the current to be infinitely narrow but otherwise to exhibit negligible spanwise or depth variation. The initial application to wave-current interactions was by *Evans* [1975], in which two regions of distinct constant currents were separated by a single vortex sheet within the deepwater regime. *Smith* [1983] extended this to water of finite depth for a jet-like current bounded by two vortex sheets. *Mei and Lo* [1984] and *Kirby* [1986] considered a similar problem to *Smith* [1983] but within the restriction of linear shallow-water wave theory. One feature of the vortex sheet models that distinguishes them from the slowly varying ones is that the reflection coefficient is expected to be appreciable.

[6] If the currents possess appreciable vertical shear, then progress can only be made if the horizontal shear is so weak as to exclude reflected waves. *Dalrymple* [1973] proposed that the kinematics may be obtained by considering the current component parallel to the direction of wave propagation. The resulting model is then two-dimensional in character but depends upon the availability of the local amplitude and wave number; local solutions may subsequently be obtained for linear waves by methods described by *Thomas and Klopman* [1997]. *Dalrymple*'s [1973] approach was also considered by *Skop* [1987] and included an implementation of the moderate current approximation (MCA) for the local wave kinematics, the MCA being applicable when the magnitude of the current velocity is much smaller than the phase speed of the waves. The principal difficulty with this model is the determination of the local amplitude and wave number for waves travelling on a slowly varying current possessing depth dependence. *Skop* [1987] suggests that conservation of wave action be employed for this purpose but incorrectly provides a version that does not take account of depth variation within the current. An approximate Lagrangian, based upon the MCA, has been proposed by *Thomas and Klopman* [1997], but without a formal derivation. A preliminary application has been given by *MacIver et al.* [2001]. However, this remains an important and unresolved problem as it is inconsistent to take account of local depth variations while neglecting global depth variations.

[7] No model includes currents with arbitrary width horizontal shear layers and which may also possess arbitrary vertical variation. Additionally, it is important to recognize that models have not been validated against experiment. *Thomas and Klopman* [1997] identified the total absence of, and subsequently the need for, quantitative experimental studies of three-dimensional wave-current interactions. Such experiments are necessary for two reasons: to produce data with which to investigate the validity of existing theoretical models and to provide an insight into the phenomena in order to direct future model developments.

[8] The present work addresses a generic problem of wave-current interaction, in which regular waves are generated on still water and encounter a narrow jet-like current at an arbitrary angle of incidence; the current may possess both horizontal and vertical shear. The current shear layers represent a strong interaction zone, from which both reflected and transmitted waves can arise; the transmitted waves then propagate on otherwise still water. It is assumed that waves always remain within the linear regime and that the bed is both smooth and horizontal; higher-order effects, such as variation in water level and wave-induced currents, are assumed negligible.

[9] This paper describes a particular experiment conducted during a short occupancy of the UK Coastal Research Facility (UKCRF) to investigate the transformation of near-linear deepwater gravity waves propagating across a narrow horizontally sheared current, a jet-like current, in water of constant depth. The experiment, described in detail in section 2, is the first attempt to assess the kinematics and dynamics of the interaction of regular waves and currents in three dimensions and an important aim is to gain an understanding of the influence of both the horizontal and vertical shear layers. The resulting data set, which includes direct quantitative measurements of the spatial variation of the velocity vector $\mathbf{u}$ and the surface elevation η, is presented in section 3. Representative theoretical models of the interaction are presented in section 4: a simple wave ray model and a new model incorporating the influence of vertical shear. A comparison of model predictions and data is presented in section 5 with results discussed and appropriate models identified in section 6, together with recommendations for further work.

2. Physical Modeling

[10] Physical modeling studies of three-dimensional wave-current interaction are rare but not unknown. Of particular note is the elegant small-scale experiment of *Hughes and Stewart* [1961] in which cylindrical capillary-gravity waves propagated on a cylindrical Couette shear flow. This experiment demonstrated the significance of the radiation stress in the energy balance equation for a gravity wave propagating on a horizontally sheared current [*Longuet-Higgins and Stewart*, 1961, 1964].

[11] Experiments at a larger, more physically realistic scale, were undertaken by *Hales and Herbich* [1972] to study the transformation of long-crested gravity waves propagating collinearly against a free turbulent jet-like current flowing through the narrow inlet of a tidal bay in a three-dimensional wave basin. Relationships for the change in wave height and length along the axis of the inlet as a function of current strength were formed, essentially considering the two-dimensional problem of waves propagating on an increasingly adverse current. In an almost identical experiment, *Ismail and Wiegel* [1983] studied the increased spreading rates of the weak jet-like current in the presence of opposing collinear gravity waves. The structure of a turbulent jet-like current emerging into a still basin, essentially an ebb flow from a tidal inlet in the absence of waves, has been studied by *Dracos et al.* [1992]. Field measurements of wave height transformation on an opposing current, whose strength varies along it axis are reported by *Lavrenov* [2003].

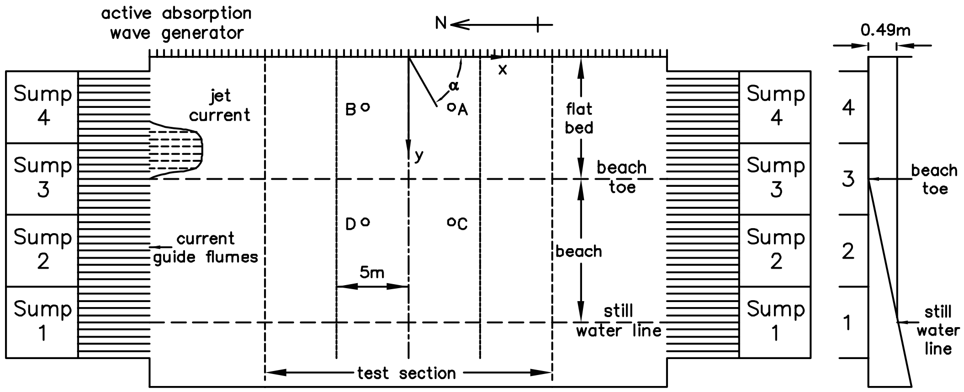

Figure 1. Schematic of the UK Coastal Research Facility.

[12] The principal reason for the absence of any quantitative experimental studies of three-dimensional wave-current interactions, as identified by *Thomas and Klopman* [1997], has been the lack of suitable facilities. However, the UKCRF is a large-scale wave-current basin incorporating a multidirectional wave generator and a refined current generation system, making it an ideal facility for the study of three-dimensional wave-current interactions.

2.1. UK Coastal Research Facility

[13] The UKCRF is specifically designed to provide a controlled environment in which coastal processes can be simulated at a physically meaningful scale. This facility measures 54 m by 27 m overall and is shown in schematic form in Figure 1. The internal dimensions of the rectangular basin measure 36 m by 20 m, determined by the position of the fixed internal boundaries: the wave generator forming the eastern boundary, current inlet/outlets forming the northern and southern boundaries and the shoreline forming the western boundary. The basin bathymetry consists of a horizontal bed located between the wave generator and the toe of a 1:20 plane beach. The test section measures 20 m by 15 m and is centered about the basin centerline. For the present tests, water depth at the wave generator was 0.49 m. The general design and capabilities of the basin have been described by *Simons et al.* [1995]. Only those aspects of the tank performance relevant to the present experiment are presented here. A more complete description has been provided by *MacIver* [2001].

2.2. Wave Generation

[14] The wave generation system consists of 72 independent piston-type wave makers, each 0.5 m wide and with an active absorption system, mounted along the eastern side of the basin. The system is designed to produce monochromatic, random and short-crested wave fields at angles of incidence between ±30° to the shore normal, with periods between 0.8 s and 3.0 s and heights up to 0.25 m. For oblique wave conditions, piston stroke is reduced at one end of the basin and the test section is restricted to a central region unaffected by sidewall effects.

2.3. Current Generation

[15] Current generation is controlled using four independent variable-speed reversible pumps, linking pairs of sumps marked sump 1 to sump 4 in Figure 1. Each pump forms part of a closed loop, drawing from and discharging into a dedicated sump situated along the northern and southern side of the basin; water drawn from sump 2 at the downstream boundary is discharged into sump 2 at the upstream boundary. This arrangement is only suitable for creating shore-parallel flows, for which the cross-shore distribution of the current at the downstream boundary is essentially similar to that at the upstream boundary.

[16] The discharge from (or into) each sump into (or from) the basin is controlled by ten 0.5 m wide drowned undershot sluice gates and associated guide flumes. This allows fine tuning of the cross-shore current profiles. Each pump has a maximum volume flow rate of approximately 0.34 m^3 s^{-1}, producing a depth-averaged velocity of approximately 0.14 m s^{-1} in a water depth of 0.49 m when each sluice gate is set at the same aperture. Varying the sluice gate apertures within a sump creates a nonuniform cross-shore profile with increased local flow rates.

2.4. Experimental Design

[17] The choice of experimental conditions demanded a balance between the need to produce significant wave refraction and the operational range of the experimental facility. Wave ray theory indicates that waves of shorter period exhibit a greater degree of refraction for a given current strength and angle of incidence. A greater degree of refraction is also achieved with larger initial angle of incidence for a given current strength and wave period, and with a stronger current for a given wave period and angle of incidence. Thus a short-period wave, at a relatively large angle of incidence and current strength, was chosen. However, this choice was subject to the constraints imposed by the characteristics and design of the UKCRF.

[18] The tests were carried out with a wave of 0.8 s period, amplitude of 0.0154 m, propagating at ±30° to the shore normal. In 0.49 m water depth, linear wave theory predicts a wavelength of 0.995 m. These conditions reduced the spurious wave generation associated with a multielement wave generator to an acceptable level [*Sand and Mynett*, 1987]. The wave is weakly nonlinear, with the ratio of second-order to first-order components of surface elevation amplitude being 5%. With k and h denoting wave number and water depth, respectively, the corresponding value of kh = 3.09 lies on the boundary between deepwater and intermediate depth conditions and is susceptible to Benjamin-Feir instabilities, which occur for kh > 1.36.

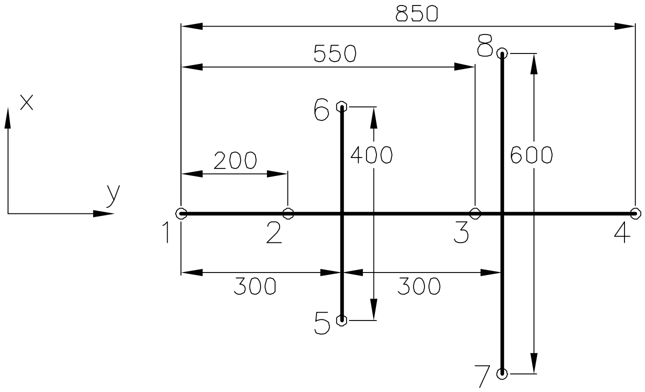

Figure 2. Wave probe array. The basin coordinate axis is included to indicate the array orientation. Dimensions are in millimeters.

However, small-amplitude waves are less prone to the instability; *Lake et al.* [1977] did not encounter instabilities for deepwater waves when $ak < 0.1$, arguing that viscous dissipation suppressed the growth of energy in the sideband frequencies for these low-energy waves. Although the *Lake et al.* [1977] study was restricted to two dimensions, their conclusion is deemed applicable to the present study, where ak is slightly smaller than 0.1.

[19] Ideally, the jet-like current created for the experiment would vary only in the spanwise direction. However, such behavior is practically unattainable as a plane turbulent jet is naturally inhomogeneous in both streamwise and spanwise directions. The evolution of a bounded plane turbulent jet, in the absence of any external influences, passes through several stages [*Dracos et al.*, 1992]. At streamwise distances from the jet source of more than ten times the fluid depth, large two-dimensional quasiperiodic vortical structures appear within the jet giving it the appearance of a staggered vortex street surrounding a meandering flow, although such features did not have a significant effect on the self-preserving form of the mean streamwise velocity. The jet-like current generated in the UKCRF is not a true free jet as its evolution is subject to the external influence of the pressure gradient caused by the extraction of the current at the downstream boundary of the basin. This suppresses the natural tendency of a jet current to slow and spread, to some degree, thus maintaining a greater uniformity in the streamwise direction. Although some broadening of the current was accepted as inevitable, the centerline of the current was required to remain parallel to the wave generator along the length of the basin.

[20] Generating the current over the horizontal bed allowed measurement of current-induced wave transformation in isolation from depth refraction effects. Maintaining regions of still water between the current and the wave generator and between the current and the foot of the spending beach allowed the incident, reflected and transmitted wave properties to be established in the absence of any current, shoaling, or depth refraction effects. To encourage the early development of a self-preserving form, the jet current was introduced into the basin with a shaped profile 4 m wide, spanning eight current guides, consisting of a central section of uniform flow, 2 m wide, and with the flow decaying in a Gaussian manner over a meter on either side. Positioning the current across the boundary between the two offshore sumps, sumps 3 and 4 in Figure 1, doubled the available discharge and so increased the maximum attainable current strength and enhanced the horizontal shear. Preliminary tests identified sluice gate aperture settings that resulted in a shore-parallel flow with minimal recirculation within the basin. The long-shore current induced by the breaking process at the head of the beach was recirculated through sump 1.

2.5. Measurement System

[21] The coordinate system chosen for the experiment takes the x axis parallel to the wave generator, the y axis as the basin centerline, and the z axis to be in the vertical direction, measured positive upward from the bed (see Figure 1).

[22] Measurements of the water surface elevation and flow velocity were made at locations on a spanwise section across the jet current. The main measurement section was located on the basin centerline ($x = 0$). Two secondary measurement sections were located five meters either side of this, as shown in Figure 1. Surface elevation measurements were made with surface-piercing resistance-type wave probes. Eight wave probes were mounted on the instrument traverse in a fixed-geometry array (Figure 2), permitting rapid mapping of surface elevation across the measurement section.

[23] Velocity measurements were made with acoustic Doppler velocimeters (ADVs). Three ADVs were mounted from the wave probe array, such that the sample volumes were located directly beneath a wave probe, providing collocated measurements of surface elevation and velocity. The ADVs were orientated to minimize flow interference for a given test condition. Measurements were made with the array positioned at 11 locations across the main section, extending from the offshore limit of motion of the instrument bridge to just onshore of the beach toe, and at four vertical elevations. This gave velocity measurements at a total of twelve elevations through the water column at each location across the main section. The position of each measuring station from the mean position of the wave makers and the notation employed for each is given in Table 1. An additional four wave probes were permanently deployed from tripods, two offshore and two onshore of the jet current to monitor the incident wave and the transmitted wave conditions.

2.6. Experimental Procedure

[24] Surface elevations and velocities were recorded for the current alone (the JET condition), the wave alone at 60°,

Table 1. Position of Measurement Stations on Basin Centerline

Station	y, m
A	3.39
B	3.89
C	4.45
D	4.89
E	5.39
F	5.89
G	6.39
H	6.89
I	7.39
J	8.39
K	9.39

90° and 120° incidence (WAF, WAN and WAO conditions, respectively) and the combined wave and current (WCF, WCN and WCO conditions, respectively). Each traverse of the measurement section was made with the wave probe array set at one of four vertical positions. The sampling frequency was 50 Hz.

[25] The current velocity at a particular location exhibited temporal fluctuations consistent with the features observed by *Dracos et al.* [1992]. However, repeatable estimates of the mean velocity were established from samples with 10-min durations. Consequently, this duration was used for any test involving the current. For wave alone tests, a sample of 5-min duration, corresponding to 375 wave periods, was used.

[26] At the start of each test, a period of time was allowed for the flow to reach a stable condition prior to measurement. A delay of 20 min was used in tests involving the current. This was reduced to 15 min for wave alone tests.

3. Experimental Considerations and Results

[27] A detailed study of the current alone condition, and the wave alone condition, was considered essential. Only with a clear understanding of the behavior of these basic conditions in the facility can the interaction phenomena in the combined conditions be fully understood and modeled.

3.1. Current Alone

[28] The generation of the current is one of the most important and novel components of the experimental work. For this reason, considerable attention was focused upon the current-alone case with regard to profile form and physical stability. *Tennekes and Lumley* [1972] proposed that the spanwise profile of a fully developed turbulent plane jet can be described by

$$\frac{U(y)}{U_0} = \mathrm{sech}^2\left[\frac{\xi}{\sqrt{2}}\right],$$
$$\frac{V(y)}{U_0} = C_b\left\{-\frac{1}{2}\tanh\left[\frac{\xi}{\sqrt{2}}\right] + \xi\,\mathrm{sech}^2\left[\frac{\xi}{\sqrt{2}}\right]\right\} \tag{1}$$

for the time-averaged streamwise and spanwise velocity components, where $\xi = (y - y_0)/b_0$ is a dimensionless spanwise coordinate, y_0 is the position of the jet current centerline, b_0 the velocity half-width and C_b is the linear rate of increase in velocity half-width. This profile was obtained from consideration of the streamwise momentum and continuity equations. A slight variant of (1) has been presented by *Dracos et al.* [1992]

$$\frac{U(y)}{U_0} = \exp\left[A\xi^2\right],$$
$$\frac{V(y)}{U_0} = C_b\left\{-\frac{1}{2}\int_0^{\xi}\exp\left[A\xi^2\right]\mathrm{d}\xi + \xi\exp\left[A\xi^2\right]\right\}, \tag{2}$$

where $A = \ln(0.5)$ and C_b was observed to be approximately 0.1. In the present case, the jet is not plane since there is an expected vertical variation in the current profile and the x variation does not correspond to a free jet. However, the representations (1) and (2) would be expected to provide good approximations to the spanwise variation of the depth-averaged velocity components at a fixed value of x.

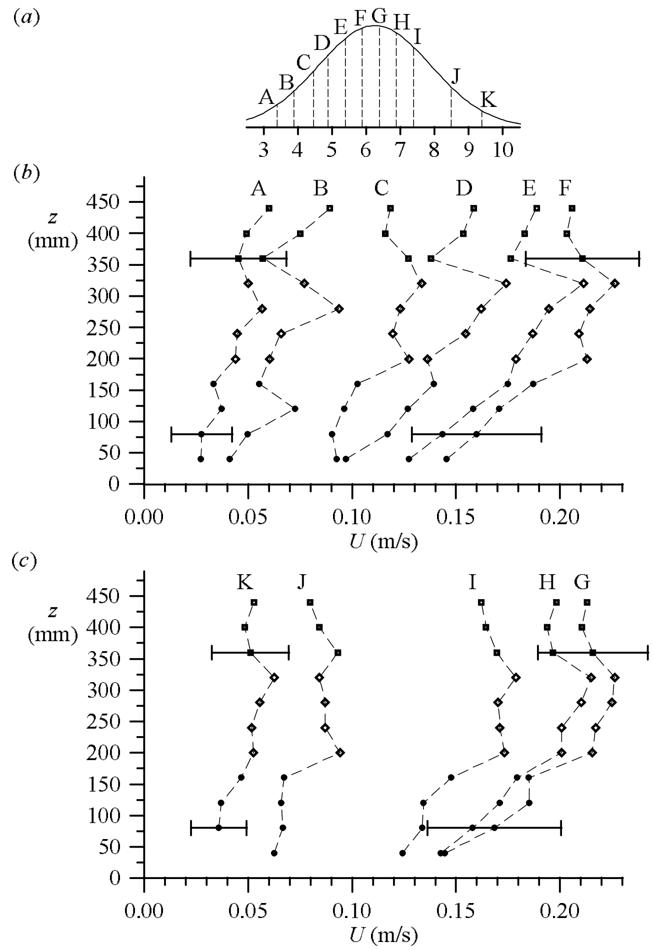

Figure 3. Vertical profiles of the mean streamwise velocity at measurement locations across the jet. (a) Schematic showing measuring positions in Table 1, (b) points A–F, and (c) points G–K. Symbols are as follows: circles, acoustic Doppler velocimeter ADV0; diamonds, ADV1; and squares, ADV2. Error bars denote the standard deviation of the velocity. Dashed lines are to aid identification of the profiles.

[29] Measured vertical profiles of the time-mean streamwise velocity, at each of the 11 measurement locations across the current on the basin centerline, are presented in Figure 3. A particular feature observed in several of the profiles are data that differ significantly from the general trend within that profile, for example, profile B. This is attributed to occasional small lateral movements of the jet current. The data presented in Figure 3 can also be viewed as a sequence of horizontal profiles at several water depths. Four such profiles are shown in Figure 4 together with a least squares fit of (1). In each case the fit is reasonable, providing a good analytical approximation to the data. The variation in depth is also clearly exhibited. As each horizontal profile is well fitted, then the depth-averaged streamwise profile $\overline{U}$ should be of a broadly similar form.

[30] The evolution of the streamwise and spanwise depth-averaged current profile between the measurement sections is shown in Figure 5. It is clear that the streamwise velocity $\overline{U}$ is predicted well by (1) and (2) at each stage across the full width of the current. The largest relative errors occur

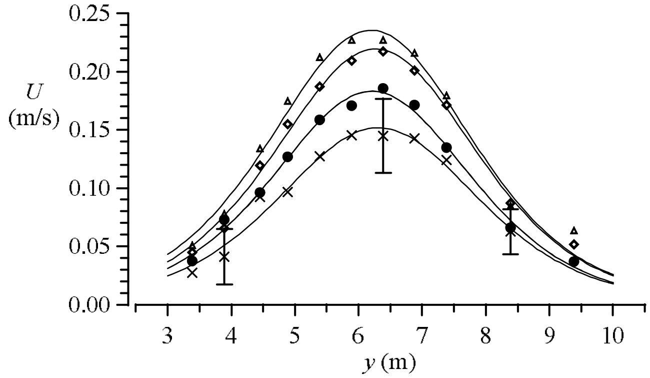

Figure 4. Representative horizontal streamwise velocity profiles, extracted from Figure 3, at four elevations: z = 40 mm (crosses), z = 120 mm (circles), z = 240 mm (diamonds), and z = 320 mm (triangles).

near the edges, an observation consistent with the findings of *Tennekes and Lumley* [1972]. The expected characteristics of a free turbulent jet flow are reproduced: the current slowing and spreading with increasing streamwise distance. The relevant parameters for the fitted profiles are given in Table 2. The current remains shore parallel through the test section, as indicated by the current centerline parameter y_0. Visual evidence from float tracking tests confirmed this characteristic and indicated that the jet current remained shore parallel over the majority of the basin.

[31] The trend of the measured spanwise velocity $\overline{V}$ also agrees with (1) and (2) although at each section $\overline{V}$ appears to be offset by an offshore flow of approximately 4 mm s^{-1}

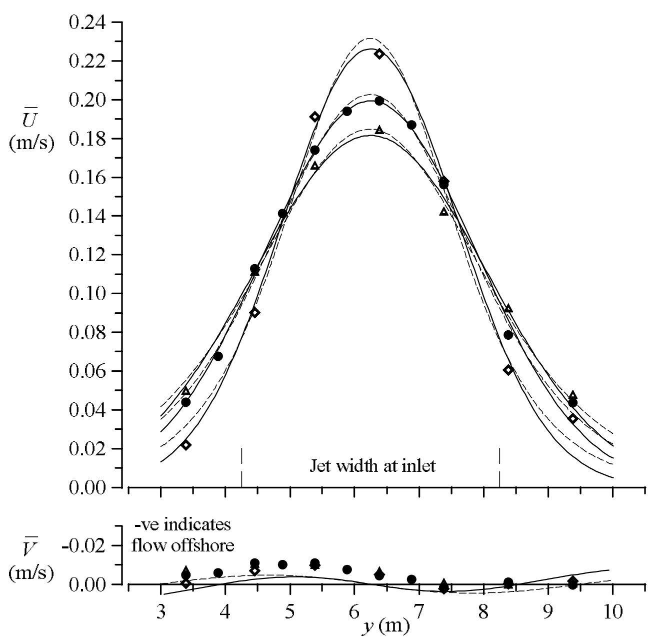

Figure 5. Development of depth-averaged horizontal current velocity components $\overline{U}$ and $\overline{V}$ through the test region. Symbols for data are as follows: diamonds, 5 m upstream; circles, centerline; and triangles, 5 m downstream. The fitted functions are equation (1), dashed line, and equation (2), solid line.

Table 2. Parameters for the Spanwise Variation of the Mean Depth-Averaged Streamwise Jet Current Velocity, Obtained From a Least Squares Fit to Equations (1) and (2)

	sech^2 Profile, Equation (1)			Gaussian Profile, Equation (2)		
Section	U_0, m s^{-1}	b_0, m	y_0, m	U_0, m s^{-1}	b_0, m	y_0, m
Upstream	0.232	1.732	6.240	0.226	1.603	6.247
Centerline	0.203	2.219	6.240	0.199	1.941	6.249
Downstream	0.185	2.353	6.236	0.182	2.143	6.248

across the entire measurement section. Such an offset is inconsistent with instrument misalignment, is unlikely to be a basin effect, as observation indicated the current to be shore parallel, and is most likely an artifact of the ADV system. It is important to recognize that $|\overline{V}|$ is very much smaller than $\overline{U}$ over the significant part of the jet and the apparent discrepancy does not warrant further attention.

[32] As the jet was turbulent, the mean flow was expected to be disturbed by eddies at a variety of length scales. In particular, large-scale vortical structures observed by *Dracos et al.* [1992] were anticipated. Velocity time series, measured near the centerline of the mean current and at approximately mid depth, indicate the presence of both long- and short-period disturbances. These are shown in Figure 6. The low-frequency part of the energy density spectra associated with the time series indicates fluctuations in both the streamwise and the spanwise velocity components, albeit at different timescales. For the streamwise velocity, the dominant fluctuation has a period of approximately 300 s, whereas the spanwise component displays a dominant period between 55 s and 75 s. The streamwise component also exhibits fluctuations at the shorter scale but these are less pronounced than in the spanwise case. The absence of similar periodic fluctuations in the vertical velocity spectrum indicates that the features are essentially two-dimensional in character, contained in the horizontal plane. Although not presented, it was also found that similar characteristics occurred at the edge of the current but with a much reduced magnitude.

[33] An estimate of the length scale of the turbulent eddies in the jet current can be achieved by invoking the hypothesis of frozen convection [*Taylor*, 1938]: temporal variation is interpreted as the convection, at some mean velocity, of a stationary spatial variation. The observations of *Dracos et al.* [1992] suggest that the fluctuations in the spanwise velocity, at locations on the periphery of the current, will be due to the convection of eddies past the measurement location at the mean streamwise velocity. The spanwise velocity frequency spectrum at the farthest offshore location on the basin centerline has a peak frequency of 0.0183 Hz (55-s period), while the mean depth-averaged streamwise velocity is 0.045 m s^{-1} (see Figure 5). Applying Taylor's hypothesis yields an estimate of approximately 2.44 m for the length scale of this eddy, comparable to the length scale of the shear layer. The peak energy equates to an angular velocity of approximately 0.01 m s^{-1} for the eddy. It should be noted that a resolution of 0.005 Hz in the frequency spectrum means the peak spectral estimate corresponds to a length scale in the range 2.15 m to 2.83 m.

[34] The eddy identified in the spanwise velocity frequency spectrum appears as the smaller peak in the streamwise

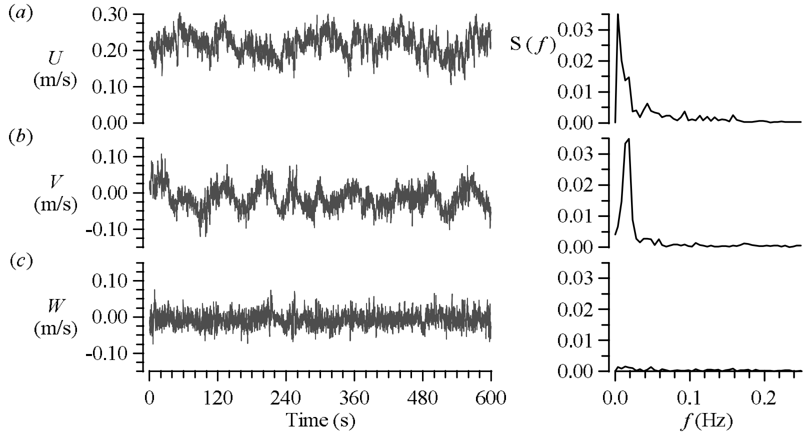

Figure 6. Time series and low-frequency detail of the energy density spectrum of the orthogonal velocity components measured near the centerline of the mean jet current, station G. Measurements were made at approximately mid depth, z = 240 mm. Resolution of spectra is 0.005 Hz.

velocity spectrum. The peak frequency corresponds to a 300 s period and is attributed to a variability in the pump output. It does not correspond to any mode of basin seiching.

3.2. Wave Alone

[35] Oscillatory components of measured quantities were determined through ensemble averaging techniques, using a static wave probe sited on the flat bed, seaward of the current as the reference signal (probe A or B in Figure 1).

3.2.1. Surface Elevations

[36] The immediate tasks, prior to the inclusion of the current, were to investigate the variability of the wave profile throughout the tank, determine the strength of reflections from the beach and to establish a generic surface profile for the wave-alone case. As stated in section 2.6, the record length in these tests corresponded to 375 wave periods. It should also be noted, as discussed in section 2.4, that there is no evidence of deepwater instability for the amplitude and frequency chosen.

[37] The wave generated in the basin was found to be temporally stable at any particular location. However, the spatial variation of wave height along the basin centerline displayed a modulation pattern inconsistent with simple reflection of the incident wave from the beach; for example, the normal incident condition exhibited a regular modulation of approximately 1.5 m, rather than the anticipated standing wave pattern at half the incident wavelength. The cause was identified as spurious disturbances originating from the guide flumes along the basin sidewalls; diffraction effects at the guide flumes produce a wave propagating radially out from the corner between the guide flumes and the wave generator at the same frequency as the test wave. This hypothesis was tested by modeling the surface elevation $\eta\,(x, y, t)$ along the centerline by the simple representation

$$\eta(y,t) = a\cos[(k\sin\alpha)y - \omega t] + \sum_{i=1}^{N} a_i \cos[(k\sin\alpha_i)y - \omega t + \phi_i], \tag{3}$$

where (a, k, α) and $\{(a_i, \alpha_i, \phi_i), i = 1, \ldots, N\}$ describe the primary wave and spurious waves respectively. The observed wave height modulation could be reproduced using $N = 2$ for the normal incidence condition and $N = 3$ for the oblique incidence conditions. Table 3 presents the parameters obtained from a least squares regression of the modulus of (3) to the wave height data of the three wave alone conditions. The inherent symmetry within the WAN condition and between the WAF and WAO conditions is reflected in the spurious wave parameters. The WAN condition yields two spurious waves that are mirror images about the basin centerline. The spurious waves of the WAF and WAO conditions are mirror images of each other. The first spurious wave for the oblique conditions corresponds to the WAN condition spurious wave. The origin of the other two, one at normal incidence and one at approximately 45° to the normal, are thought to be associated with the generation of oblique waves by a multielement wave generator [*Sand and Mynett*, 1987]. Although not shown in Table 3, the fit predicts the wave number to within 1% relative error. Further details are provided by *MacIver* [2001].

[38] The nature of oblique wave generation, namely, paddle stroke reduction and an inherent wave shadow zone,

Table 3. Fitted Parameters of Wave Height Modulation in Wave-Alone Cases for Normal (WAN), Following (WAF), and Opposing (WAO) Incidence

	WAN			WAF			WAO		
	a, m	α, deg	ϕ, deg	a, m	α, deg	ϕ, deg	a, m	α, deg	ϕ,
Test wave	0.0159	90.0	-	0.0160	60.0	-	0.0155	120.0	-
Spurious 1	0.0007	20.0	83.8	0.0005	21.2	189.9	0.0005	152.9	349.8
Spurious 2	0.0007	160.0	83.8	0.0026	90.5	191.5	0.0044	89.5	272.9
Spurious 3	-	-	-	0.0020	131.5	324.0	0.0036	44.6	282.5

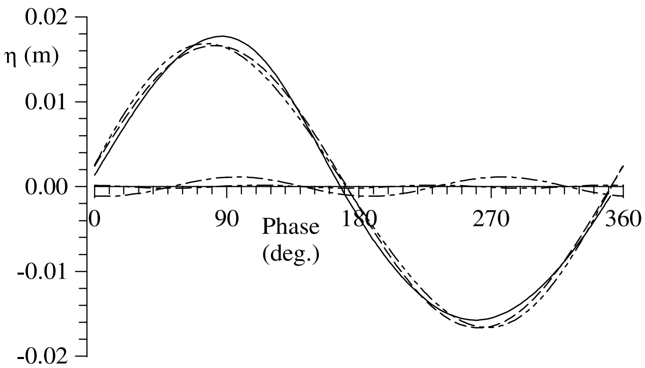

Figure 7. Ensemble-averaged surface elevation profile for wave obliquely incident at 60°. The first three harmonic component profiles and a second-order Stokes wave profile are also shown: ensemble average, solid line; first harmonic, dashed line; second harmonic, long and one short dashed line; third harmonic, long and two short dashed line; and Stokes second order, long and three short dashed line.

significantly reduces the possibility of spurious wave generation at the guide flumes; however, the observed wave height modulation indicates the presence of one or more spurious waves. The nature of the modulation along the centerline differs from that observed for normal incidence; there is a dominant longer-modulation wavelength, with other secondary influences. The outcome of fitting the modulus of (3), with $N = 3$ and the parameter α fixed at the appropriate nominal value, to the following (WAF) and opposing (WAO) oblique wave conditions is shown in Table 3. The symmetry of the these conditions is evident. The first spurious wave for both the WAF and WAO condition corresponds to one of the spurious components in the WAN condition, with the identified component being the one propagating in the same x direction as the generated wave. At first sight, the amplitudes of the second and third spurious waves look alarming, being a little below 30% of the incident amplitude in the largest case. However, because of the directionality and phase of the components, the net result is similar to the WAN case, with a wave height variation of 9% about the mean. An interpretation of the angles of the second and third spurious waves is not easy but it should be noted that (3) only represents a fitting to the wave elevation and does not attempt to include all possible wave components. As in the case of normal incidence, the wavelength is predicted to a relative accuracy of 1% in comparison to the value from the linear theory.

[39] The beach reflection coefficients could only be determined with confidence by suppressing the spurious waves described above. This was achieved by reducing the stroke of those paddle elements considered responsible for the generation of the spurious wave effects. Although this does not result in long-crested waves throughout the tank, the waves are sufficiently long-crested in the test region to enable the beach reflection coefficients to be estimated. These were obtained using the least squares optimization method of *Isaacson* [1991], with the reflection coefficient found to lie between 1% and 4% for both normal and oblique incidence.

[40] An ensemble-averaged surface elevation for the test wave at 60° incidence is shown in Figure 7, together with the first three harmonic components and a Stokes second-order prediction based upon the local wave height. It is interesting to note that the profile does not correspond to that of a linear wave, neither is it described particularly well by a Stokes second-order prediction; the harmonic components of a Stokes wave would be in phase and this is not the case. The measured second-order harmonic amplitude is approximately 7% of the first harmonic amplitude, which is somewhat larger than the expected bound Stokes second-order amplitude. The difference is attributed to the presence of a free second harmonic resulting from the use of a piston-type wave maker to generate essentially a deepwater wave. This is supported by the phase difference between the harmonic components. Thus the incident wave is not fully monochromatic and is weakly nonlinear, although the magnitude of its first harmonic is consistent with linear theory.

3.2.2. Velocity Measurements

[41] A typical example of the behavior of the ensemble-averaged horizontal components of the wavelike velocity vector ($\widetilde{u}$, $\widetilde{v}$, $\widetilde{w}$), and its first harmonic representation, is presented in Figure 8a for measurements at one vertical elevation and at a number of locations across the basin centerline. An estimate of the propagation direction can be established from the vectors, either from the linear least squares regression to each ensemble vector or from the alignment of the major axis of the first harmonic vector.

[42] The open nature of the velocity vector ellipse is further confirmation of the presence of wave components additional to the test wave. However, as the ellipses are not regular, it suggests that one or more of the velocity components differ in frequency from that of the test wave. Inspection of the higher harmonics of the ensemble average velocity reveals a small, yet significant, fourth harmonic component whose magnitude and direction varies little between measurement locations. This is attributed to wave induced oscillation of the instrument support. Despite the open character of the ellipses, both the least squares method and the first harmonic vector method provide excellent agreement for the predominant wave direction.

[43] Figure 8b shows that the mean velocities for wave-alone conditions are generally negligible, though there are one or two anomalous points. Such measurements were made following the action of bringing sediment back into suspension, in order to improve the signal quality of the ADVs. The observed mean flows are most likely to be residual currents produced by the agitation process.

[44] The vertical variation in the magnitude of the first harmonic of the resultant horizontal and vertical velocity vectors is predicted in the linear theory by

$$\sqrt{\widetilde{u}^2 + \widetilde{v}^2} = a\omega \,\frac{\cosh k(z+h)}{\sinh kh}\;, |\widetilde{w}| = a\omega \,\frac{\sinh k(z+h)}{\sinh kh}.$$

In applying the formulae, both the amplitude a and wave number k must be determined from the experimental measurements. The local wave amplitude was measured immediately above the location of the velocity profile and the wave number was determined from the rate of increase of wave phase in the WAN case. Excellent agreement was found at all measuring stations along the basin centerline for all three wave-alone conditions. Very minor discrepancies

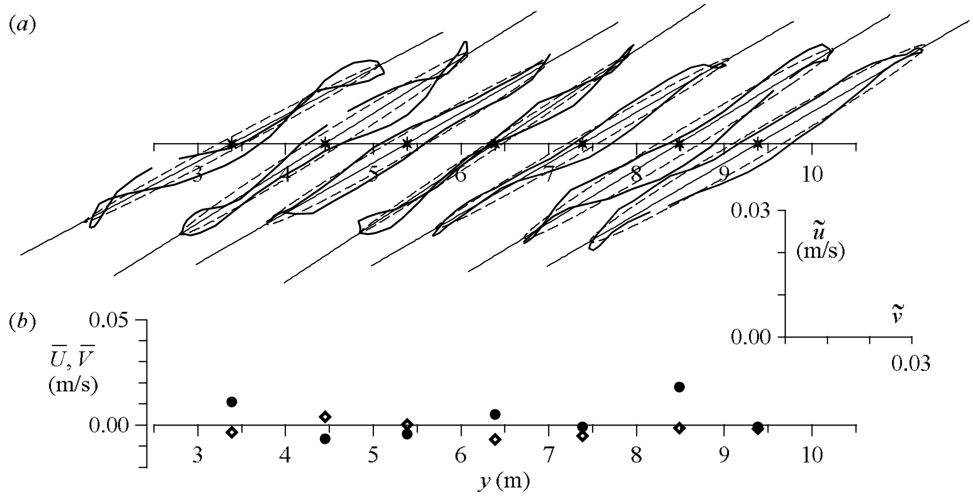

Figure 8. Horizontal velocity components for an obliquely incident wave of 60° in the absence of the current at points A, C, E, G, I, J, and K of Table 1. (a) Velocity vector for oscillatory components $\tilde{u}$ and $\tilde{v}$ at z = 310 mm: ensemble averaged (solid line) and first harmonic vector (dashed line). (b) Depth-averaged mean components: $\overline{U}$ (circles) and $\overline{V}$ (diamonds).

between prediction and measurement occurred near to the free surface on some of the profiles and attributed to higher-order terms that contribute to the total first harmonic contribution. However, their influence is extremely small.

3.3. Wave and Current

[45] Attention is concentrated upon the changes in current profiles and surface elevations resulting from the interaction; the wavelike velocity profiles are presented as part of the comparison between experiment and prediction in section 5.2.

3.3.1. Current Profiles

[46] Before studying the detailed current profiles for the three cases of WCN, WCF and WCO, it is instructive to examine the depth-averaged currents (Figure 9, with fitting parameters for the Gaussian fit (2) presented in Table 4). A comparison between Tables 2 and 4 enables the extent of any changes to be estimated.

[47] The striking feature is the lateral displacement of the current under combined conditions. This is most pronounced under the obliquely incident condition WCO, in which the current centerline is displaced more than a meter offshore at the basin centerline and also appears to be flowing slightly offshore through the test section. Such a large displacement prevented measurements at the offshore edge of the current. For the WCF condition, the displacement is approximately 0.3 m onshore at the basin centerline, with a small offshore deviation from the intended shore-parallel direction through the test section. In the normally incident WCN case, there is a smaller change, with the centerline being within 0.1 m of the JET condition.

[48] In addition to the lateral displacements, the characteristic parameters of the mean flow for the combined wave-current conditions, and the current alone condition, all differ from each other, although variations are relatively small. All three combined conditions exhibit a small reduction in centerline velocity, of less than 7.5% of the current-alone centerline velocity, with the WCF case showing least variation. The WCN and WCF conditions possess a smaller velocity half-width than the current-alone, indicating a narrower jet current, while the opposing WCO condition possesses a larger half-width. All values differ by less than 6% of the current-alone half-width. The spanwise component remains small in all cases, with the most significant change being exhibited by the WCO condition and this is consistent with the changes in the streamwise component described above. An increased spreading rate and increased deceleration of centerline velocity has been observed previously for the case of a turbulent jet current in the presence of an opposing collinear wave [*Ismail and Wiegel*, 1983]. The dominant mechanism for this behavior was identified as

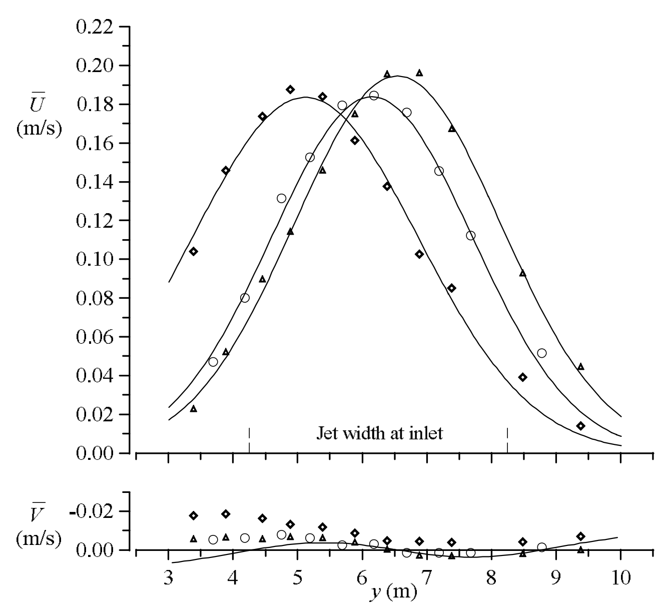

Figure 9. Depth-averaged mean velocity components $\overline{U}$ and $\overline{V}$ on the basin centerline for the combined wave-current tests: WCO (diamonds), WCN (circles), and WCF (triangles).

Table 4. Parameters for the Spanwise Variation of the Mean Depth-Averaged Streamwise Current Velocity in the Presence of Waves for Normal (WCN), Following (WCF), and Opposing (WCO) Incidence[a]

	WCN			WCF			WCO		
Section	U_0, m s^{-1}	b_0, m	y_0, m	U_0, m s^{-1}	b_0, m	y_0, m	U_0, m s^{-1}	b_0, m	y_0, m
Upstream	-	-	-	0.221	1.602	6.441	0.215	1.711	5.706
Centerline	0.186	1.831	6.152	0.195	1.888	6.545	0.184	2.060	5.118

[a]The fitting is via the Gaussian profile, equation (2).

the divergence of the wave momentum flux arising from wave refraction about the current centerline.

[49] The vertical profiles at the approximate centerlines of each current are shown in Figure 10 and they are based upon the nearest measurement point from Table 1 and Figure 9. In two-dimensional wave-current interactions the current profile adjusts itself differently for following and opposing waves. *Ismail* [1984] suggests that good approximations to the kinematics of the following and adverse currents, within the linear wave regime, can be obtained by a uniform current and constant vorticity models, respectively. Experimental support is provided by *Kemp and Simons* [1982, 1983] and *Klopman* [1994], with theoretical confirmation of the form of the stable profiles presented by *Groeneweg and Klopman* [1998]. These conclusions do not hold for obliquely incident waves in three dimensions, when compared to the current-alone case. Figure 10 shows clearly that there is a reduction in the mean flow in the upper third of the water column for both following and opposing obliquely incident waves. In the lower two thirds of the profile, there is an increase and reduction for the following and opposing cases respectively but the basic structure is similar. Perhaps, even more surprisingly, the presence of a normally incident wave field changes the current profile so as to become almost linear.

[50] The vertical structures of the streamwise velocity profiles for the three combined conditions are shown in Figure 11. Figures 11a–11c are intended to illustrate the variation, or otherwise, of the vertical profile across the jet. Attention is restricted to half profiles of the jet, with the offshore portion being presented for the WCN and WCF conditions. The onshore portion is shown for the WCO condition, since Figure 9 has already shown that the offshore portion is not complete in this case. Profiles at points on opposite sides of the current were found to be broadly similar, because of symmetry. Some minor differences were encountered near to the surface at corresponding pairs of measuring points, and possibly at other comparable pairs, but the most important changes are contained in

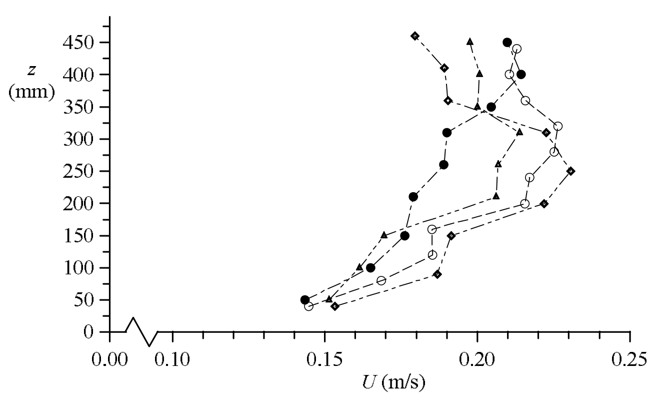

Figure 10. Vertical profiles of the streamwise current component at the approximate centerline of the jet for all measured conditions: JET (open circles), WCN (solid circles), WCF (diamonds), and WCO (triangles). Dashed lines are to identify individual profiles.

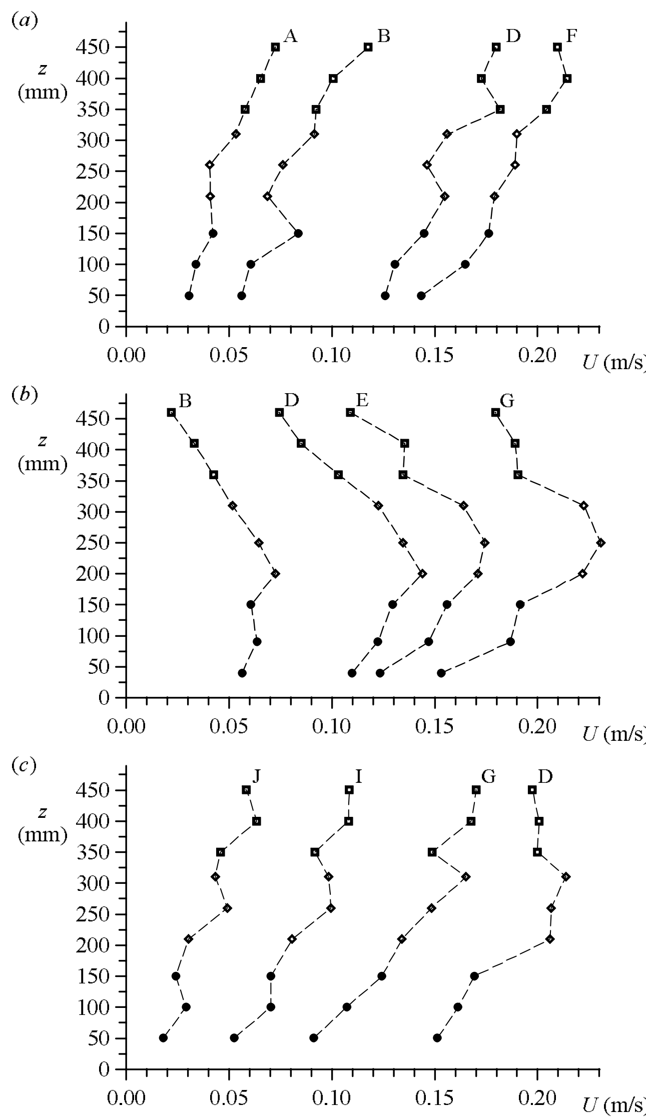

Figure 11. Vertical profiles of the streamwise current velocity at locations across the jet current under combined wave-current conditions: (a) WCN, (b) WCF, and (c) WCO. ADVs are shown as follows: ADV0, circles; ADV1, diamonds; and ADV2, squares. Dashed lines are to aid identification of profiles.

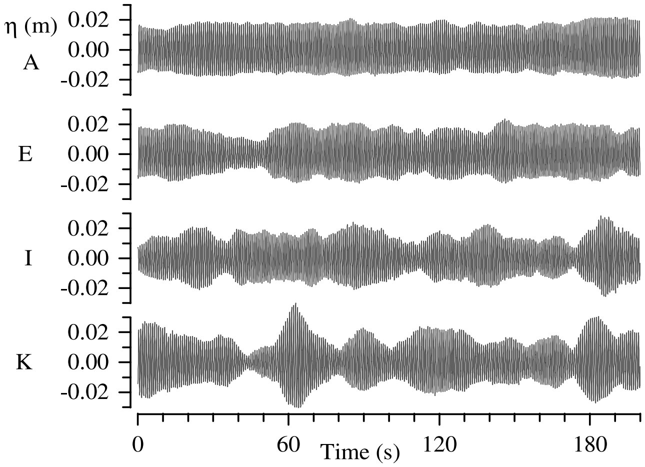

Figure 12. Surface elevation time series at uniformly spaced locations A, E, I, and K across the centerline for the WCF wave-current condition.

Figure 10. Some care is necessary when comparing Figure 11a directly with Figure 3 or the other profiles in Figure 11, since not only is the jet displaced slightly by wave action but the measurement stations are displaced shoreward by 0.3 m by choice of measuring system.

[51] It is clear that the global vertical variation in the current profile is strongly dependent upon the angle of incidence of the waves, relative to the current-alone profiles. Figure 3 shows that the maximum current is a little above mid depth across the jet, with some indication of surface streaming most likely a tank effect. For the WCF condition in Figure 11b, the flow is strongest in the lower portion of the profile near the edge of the jet; the maximum flow point moves upward toward mid depth at the center of the jet. The opposite phenomenon occurs for the WCO condition in Figure 11c, where the maximum flow point is near to the surface at the edge of the jet and moves downward toward the center of the jet. It has previously been stated that the centerline profile for the WCN condition is essentially linear and this is the case throughout the profile. These changes in profile, which must depend upon wave-induced turbulent stresses in the flow, are the subject of further research and no attempt is made to discuss the mechanism here.

3.3.2. Surface Elevations

[52] Wave height at a particular location experienced a temporal modulation that became more pronounced with distance onshore (Figure 12), in contrast to the wave-alone condition. This is a purely spatial effect, with no evidence to suggest that the degree of modulation increases over time at any particular location.

[53] The spectra for the first and last stations in Figure 12, which are the least and most variant, respectively, together with the spectra in the corresponding wave-alone cases, are shown in Figure 13. In the absence of the current, the spectrum is sharply peaked at the fundamental frequency and its harmonics. When the current is present, the peaks are broadened and the background noise level is considerably increased, almost obscuring the peaks of the higher harmonics. As expected, this is most pronounced at station K but it is also clearly visible at station A. A consequence of this modulation is an increased variability in the zero-crossing wave period, relative to that observed in wave-alone conditions. Although this increased variability has only a small effect on the recovered mean wave period, it does result in an underestimate of the amplitudes of oscillatory quantities recovered by ensemble averaging, as the basic time series are no longer phase locked exactly. However, the majority of the wave energy remains concentrated in a narrow band about the peak spectral frequency. Therefore, for combined wave-current conditions, the wave height was determined from the energy contained in this narrow band about the peak spectral frequency.

[54] In wave-current conditions reflected waves can occur from the beach and from both shear layers of the current. If the shear layers are sufficiently strong, it is also possible for trapped waves to exist on the current. This is considerably more difficult to analyze than the wave-alone case and a preliminary analysis in the linear regime has been provided by *Thomas* [1999]. Possible reflections are not easy to estimate a priori, yet such estimates are important, as a knowledge of their magnitudes contributes to an interpretation of the experimental measurements. Surface elevation measurements nearest the wave generator for the WCN condition analyzed using the least squares optimization method of *Isaacson* [1991] yield a total reflection coefficient of less than 2%. The corresponding quantity for the WCF condition lies between 2% and 6%, which is a very slight increase over the wave-alone value, estimated previously to lie between 1% and 4%. Thus any increases over the wave alone conditions may be considered small, certainly within the bounds of experimental variability, suggesting there is no appreciable reflection at the current shear

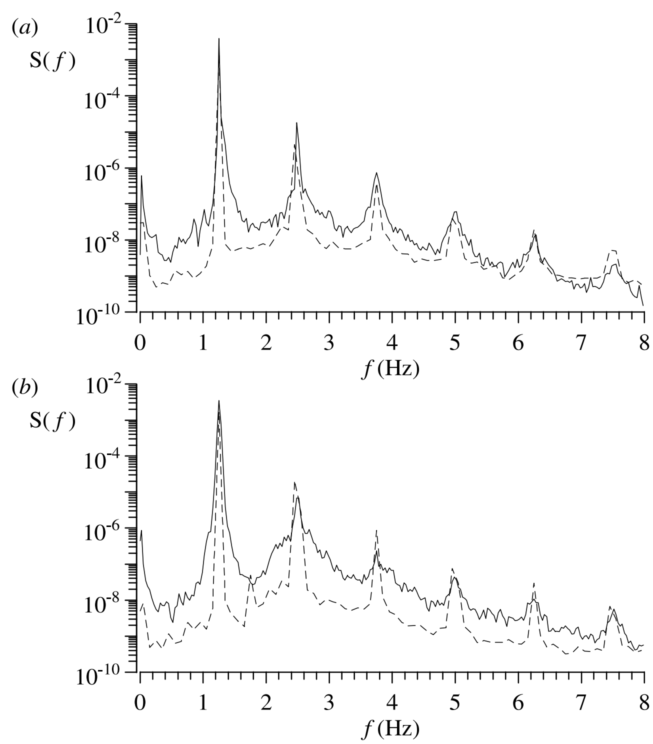

Figure 13. Surface elevation spectra corresponding to measuring stations: (a) A and (b) K in Figure 12. WCF is shown by solid line; WAF is shown by dashed line. Frequency resolution is 0.1 Hz.

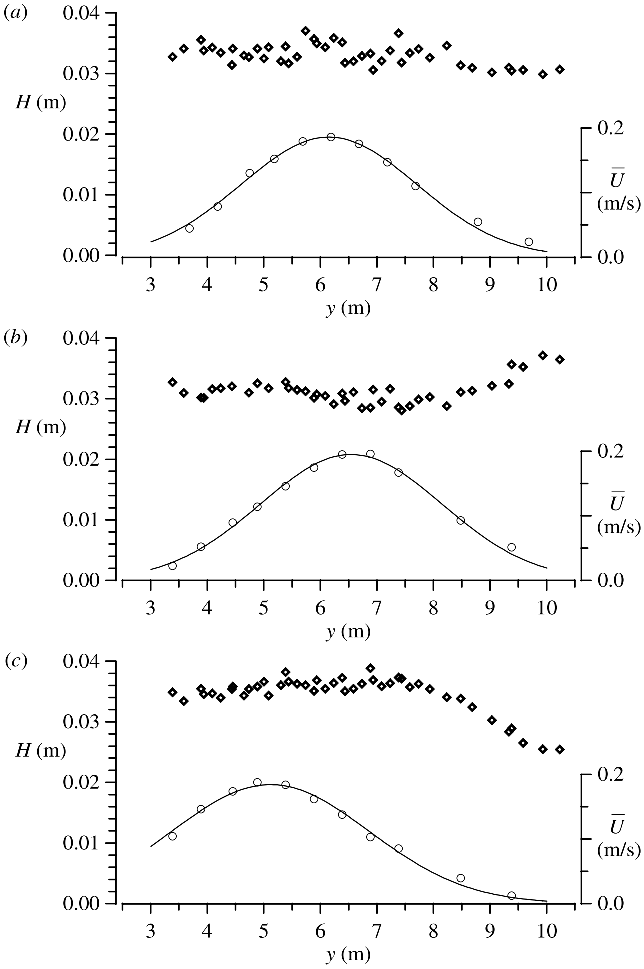

Figure 14. Variation of wave height for combined wave-current conditions: (a) WCN, (b) WCF, and (c) WCO. Wave height is shown by diamonds; streamwise current $\overline{U}$ is shown by circles.

layers. It should be noted that a similar analysis cannot be conducted for the WCO condition because the jet was offset very close to generators as shown in Figure 9.

[55] The measured wave heights for the combined conditions WCN, WCF and WCO are shown in Figures 14a–14c, respectively. The depth-averaged current profile from Figure 9 is also shown, to aid interpretation of the data. Figures 14a–14c illustrate scatter in the current region and unanticipated behavior in the region on the shore side of the current. Given that each wave height is determined as a spectral measure of a time series similar to those shown in Figure 12, a degree of scatter is to be expected. However, the greatest scatter appears to be present for the case of normal incidence and this is rather surprising, since laminar/inviscid theories suggest that waves and currents do not interact for a WCN configuration. It is possible that spurious waves play a role, as in section 3.2.1, but the degree of symmetry leading to the fitting function (3) is not present and so this cannot provide the sole reason.

[56] For normal incidence, Figure 14a shows the reduction in wave height on the shore side of the current to be uniform and approximately 4mm in magnitude, or just over 10% of the incident value. For the following wave (Figure 14b), the change is an increase of 16%. The corresponding change for the opposing wave in Figure 14c is a decrease of 21%. These changes in wave height were not anticipated. The variation of wave height in the current region is further discussed in section 5.2.2.

3.3.3. Kinematics

[57] As reflections of the primary incident wave from the beach and shear layers were not considered significant, it was feasible to study the refraction and wavelength variation by the phase analysis method of *Simons and MacIver* [2000]. Figure 15 shows the phase variation for normally incident waves in the presence and absence of the current. The straight line is the least squares fit to the wave-alone phase variation, the slope of which represents the wave number. There is a small, but consistent, difference between the WAN and the WCN conditions indicative of a refractive process. The rates of change of wave phase are initially indistinguishable at the offshore (incident) edge of the current. On the current the rate first increases then decreases corresponding to a shortening and lengthening of the wavelength. Ultimately, there is a very slight phase lag between the two conditions, although this may be associated with further interaction with secondary circulation currents. Note an inviscid/laminar model of wave current interaction predicts no interaction.

[58] The phase changes for the WCF and WCO conditions are shown in Figure 16, with the WAO data providing a reference point. Both are parallel to WAO data at the onshore and offshore edges of the current, with the variation of phase due to refraction on the current being clearly seen. The rate of increase is reduced on the current for the WCF case and increased for the WCO case, reaching a minimum and maximum respectively near the location of the maximum current strength. It should be noted that the current maxima differ in location for the two data sets. A reduction

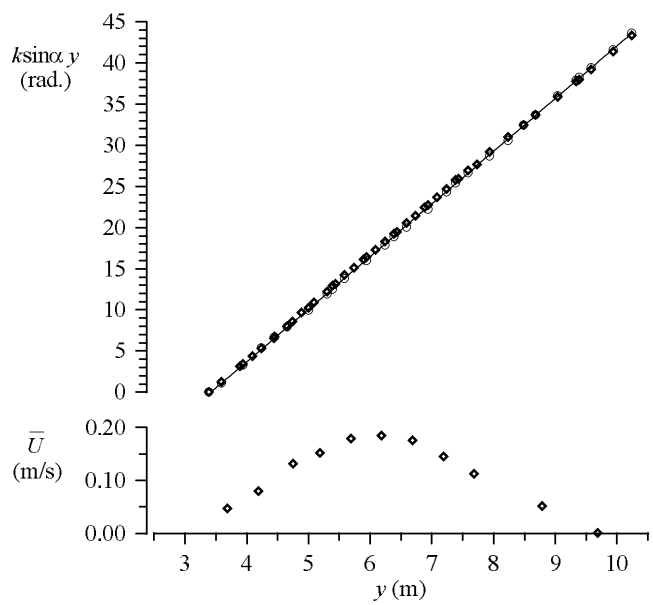

Figure 15. Variation of wave phase, relative to the first measurement point, for the WAN (circles) and WCN (diamonds) conditions. The WCN depth-averaged streamwise current profile is also shown. Line indicates least squares fit to WAN.

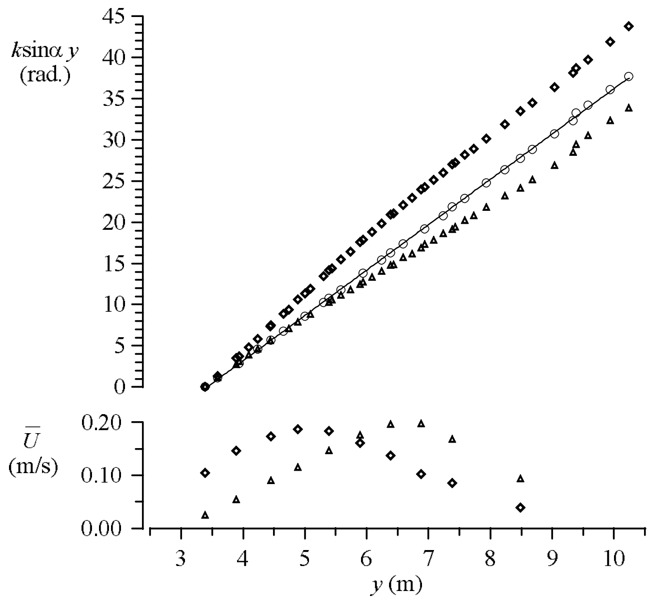

Figure 16. Variation of wave phase, relative to the first measurement point, for the WCF (triangles), WCO (diamonds), and WAO (circles) conditions. The corresponding depth-averaged streamwise current profiles are also shown. Line indicates least squares fit to WAO.

in the rate of increase is consistent with a longer wavelength and a more current parallel propagation direction, while an increase corresponds to a shorter wavelength and more current perpendicular propagation direction. This is precisely what would be expected for an obliquely propagating wave on a slowly varying current.

4. Theoretical Models

[59] Two models are presented for comparison with experimental data; the wave ray model and an extension to three dimensions of the two-dimensional averaged Lagrangian model, employing the moderate current approximation, presented by *Thomas and Klopman* [1997]. A preliminary assessment of the Mild Shear model [*McKee*, 1987, 1996] for the case of deepwater conditions WCF and WCO incident upon a depth-averaged approximation to the current in the form of (1), predicted negligible reflection coefficients. Thus, as the predictions of the Mild Shear model were indistinguishable from those of the wave ray model, it is not presented independently here.

4.1. Modeling Considerations

[60] The current is taken to be uniform in the streamwise direction but with arbitrary variation in both the spanwise and vertical directions, i.e., $\mathbf{U} = (U(y, z), 0, 0)$. It is usual in theoretical modeling to measure the vertical coordinate positive in an upward direction, with the origin at the undisturbed free surface. This convention is adopted here, in contrast to the experimental study where the coordinate origin is taken to coincide with a point on the horizontal bed.

[61] Regular waves of amplitude a_0 and frequency ω propagate unhindered at an angle of incidence α_0 over water of uniform depth h from $y = -\infty$ until they encounter the current. On meeting the current, the waves may be reflected, or transmitted into the otherwise still water beyond the current. Linear wave theory is assumed to be valid in all regions. For the specific current structure and incident wave conditions, the general formulation is best defined in terms of the wavelike pressure, as shown by *Thomas and Klopman* [1997]. However, some simplification is possible, since the x dependency in the wave description must remain unchanged from that present in the incident wave. Writing the local wave number vector as $\mathbf{k} = (k_1, k_2, 0)$, this may be described by an e^{ik_1x} factor, where k_1 is constant, so that the resulting spatial dependency is only upon y and z. If the spanwise current variation is negligible at the scale of a wave period and wavelength, i.e., $|\partial\mathbf{U}/\partial t| \ll |\omega\mathbf{U}|$ and $|\nabla\cdot\mathbf{U}| \ll |\mathbf{k}\cdot\mathbf{U}|$, then the variation can be considered as slowly varying and the current can be considered to be locally uniform. If these relations do not hold, then wave reflection must be accounted for.

4.2. Wave Ray Model

[62] The wave ray model, or WKBJ approximation, is described in detail by *Jonsson* [1990] and only the salient features will be presented here. Waves are considered locally plane, and motion is locally irrotational. The current is assumed to be uniform over depth and slowly varying in the spanwise direction. Reflection is not permitted at the current and the local wave motion is that of a linear wave on a uniform current. Conservation relations are employed to predict the changes due to refraction by the current.

[63] The local wave field can be represented in terms of a potential Φ (x, y, z, t) and surface elevation η (x, y, t) of the form

$$\begin{aligned}\Phi(x,y,z) &= \frac{ag}{\omega}\frac{\cosh k(z+h)}{\cosh kh}\cos(k_1x + k_2y - \omega t),\\ \eta(x,y,t) &= a\cos(k_1x + k_2y - \omega t).\end{aligned} \tag{4}$$

This is to be employed in conjunction with the local dispersion relation, which is implemented in the form

$$\begin{aligned}\left(\omega - k_1\overline{U}\right)^2 &= gk\tanh kh,\\ \overline{U}(y) &= \frac{1}{h}\int_{-h}^{0} U(y,z)\,\mathrm{d}z,\end{aligned} \tag{5}$$

where $\overline{U}(y)$ is the slowly varying depth-averaged current.

[64] The local wave number vector can be written as $\mathbf{k} = k(\cos\alpha, \sin\alpha, 0)$, where $k = |\mathbf{k}|$. As k_1 remains unchanged, we have

$$k_1 = k\cos\alpha = k_0\cos\alpha_0 \tag{6}$$

throughout the domain, the subscript 0 indicating incident wave conditions. The amplitude variations correspond to conservation of wave action and are usually referenced to the incident wave field,

$$\left(\frac{a}{a_0}\right)^2 = \frac{Q(k_0h)}{Q(kh)}\frac{\sin 2\alpha_0}{\sin 2\alpha}, \tag{7}$$

where $Q(kh) = 1 + 2kh/\sinh 2kh$. For given initial parameters (a_0, k_0, α_0), the local values of (a, k, α)

corresponding to a given value of $\overline{U}$ can be obtained from (5)–(7), with the local kinematics finally obtained via (4).

[65] The above description remains valid provided that caustics are not present and this imposes a limitation on the model. Caustics occur as the rays are refracted so as to become parallel to the current and can only occur in the WCF case. If U_0 is the maximum value of the jet current and caustics are predicted to occur when $\overline{U} = U_c$, then there will be no caustics if $U_0 < U_c$, one if $U_0 = U_c$ and two if $U_0 > U_c$. For deepwater conditions, as in the experimental data, the caustic occurs when

$$\frac{U_c}{c_0} = \frac{1 - \sqrt{\cos\alpha_0}}{\cos\alpha_0}, \tag{8}$$

where $c_0 = \omega/k_0$ is the phase speed of the incident waves.

4.3. Moderate Current Approximation

[66] This is an extension to three dimensions of the two-dimensional averaged Lagrangian model, employing the MCA, presented by *Thomas and Klopman* [1997]. The current may possess arbitrary vertical variation but is assumed to be slowly varying in the spanwise direction and so wave reflection is not permitted. It is assumed that the nondimensional current parameter U_0/c_0 and wave slope ak satisfy the condition $ak \ll U_0/c_0 \ll 1$ and this defines the ordering of the approximation. Although this approach has not been formally validated, it is an initial attempt to include some measure of current variation with depth into the averaged Lagrangian approach. Preliminary calculations with this model are described by *MacIver et al.* [2001].

[67] First-order variations in the wave properties, for the linear wave regime, are assumed to be described by the averaged Lagrangian

$$\mathcal{L} = \frac{\rho g a^2}{4}\left\{\frac{\left(\omega - k_1\widetilde{U}(y)\right)^2}{gk\tanh kh} - 1\right\}, \tag{9}$$

where the quantity $\widetilde{U}(y)$ is defined by

$$\widetilde{U}(y) = \frac{2k}{\sinh 2kh}\int_{-h}^{0} U(y,z)\cosh 2k(z+h)\,\mathrm{d}z. \tag{10}$$

The structure of (9) is based upon comments on the averaged Lagrangian, for linear waves, made by *Jonsson et al.* [1978], together with the dispersion relation presented by *Skop* [1987] for wave-current interactions within the MCA regime.

[68] The conservation relations for (a, k, α) are obtained from the averaged Lagrangian via

$$\frac{\partial\mathcal{L}}{\partial a} = 0, \quad k_1 = k\cos\alpha = \text{constant}, \quad \frac{\partial\mathcal{L}}{\partial k_2} = \text{constant}.$$

The first expression gives the dispersion relation

$$\left(\omega - k_1\widetilde{U}(y)\right)^2 = gk\tanh kh, \tag{11}$$

and the second corresponds to conservation of k_1, as in (6). The third expression yields conservation of wave action

$$a^2F\left(\omega, k, \widetilde{U}(y)\right)\sin 2\alpha = \text{constant}, \tag{12}$$

with the function $F(\omega, k, \widetilde{U}(y))$ given by

$$F\left(\omega,k,\widetilde{U}(y)\right) = Q(kh) + \frac{2k_1}{\omega - k_1\widetilde{U}}\left\{\left(1 - \frac{2kh}{\tanh 2kh}\right)\widetilde{U} + \frac{4k^2}{\sinh 2kh}\int_{-h}^{0}(z+h)\widetilde{U}(y,z)\sinh 2k(z+h)\,\mathrm{d}z\right\}. \tag{13}$$

The constant in (12) is best considered by reference to the incident wave field, as with (7). A direct comparison can also be made between the ray theory expression (7) and (12). For the case of a current without depth variation, (13) reduces to $Q(kh)$ and this is the wave ray model. So the terms inside the braces in (13) are a consequence of the current being permitted to vary with depth.

[69] Equations (6) and (10)–(12) provide the conservation relations for the determination of (a, k, α). The local velocity field can then be obtained via the MCA, as given by *Thomas and Klopman* [1997] or the Rayleigh model of *Thomas* [1981]. In either case the implementation will involve a numerical approach and imposition of the constraint that k_1 remains constant.

5. Comparison of Measurement and Prediction

5.1. Model Implementation

5.1.1. Current Representation

[70] A reasonable description of the basic depth-averaged current profile was given by (1) (Figure 5). However, in implementing the models of section 4 a more accurate description of the horizontal variation, and depth variation in the case of the Moderate Current Approximation model, is required. Thus a necessary task is to fit the horizontal and vertical variation of $U(y, z)$ and then obtain the depth-averaged approximating current $\overline{U}(y)$.

[71] The experimental data essentially lie on a rectangular grid which provides the basis for the description of the current. Fitting methods require that each data point is given an individual weighting; points with a good degree of confidence are given unit weighting, with lower values for points that appear less reliable or are inserted. The choice of weighting plays an important role in the fitting process. Values of the current at the free surface and at the bed are approximated by extrapolation, based on a number of the nearest internal data points and including at least one inserted point between the boundary and the nearest true data point. These additional points are given progressively lower weighting from the domain outward to lessen the reliance upon extrapolation.

[72] The jet-like character of the current requires the magnitude of U and its derivatives to tend to zero as $|y| \to \infty$, yet the numerical implementations of the models must be deployed on a finite domain. For a symmetric jet, with centerline at $y = 0$, it is sufficient to establish a finite value L such that the current and its derivatives can be considered negligibly small when $|y| > L$; clearly the smallest acceptable

L should be employed. In practice, it is necessary to determine values L_1 and L_2 from the experimental data such that $L_1 \leq y \leq L_2$ defines the y domain, with the boundary values chosen so that they correspond to regions of still water in the absence of waves.

[73] Following the usual practice for finite depth waves, the vertical variation is nondimensionalized with respect to the water depth h to give a nondimensional variable $Z = z/h$; the corresponding horizontal variation is scaled with respect to the incident wavelength λ_0 to define $Y = y/\lambda_0$. Thus the current $U(y, z)$ is considered as $\widehat{U}(Y, Z)$ on the domain $L_1/\lambda_0 \leq Y \leq L_2/\lambda_0$, $-1 \leq Z \leq 0$. Although the values of L_1 and L_2 define the numerical domain, these values may lie outside the boundaries of the experimental domain. In such cases it is necessary to insert additional points to force the fitting scheme and choose the inserted point weightings accordingly. This requires some care and the best option is generally to keep the domain as short as possible, with some experimentation in the best choice of available parameters.

[74] A number of fitting approximations to $\widehat{U}(Y, Z)$ were attempted, with the requirement that the curve fitting method had to balance numerical exactness with a necessary degree of smoothing. Ultimately, a mixed format representation of exponentials and other matching functions was chosen, with the structure

$$\widehat{U}(Y,Z) = U_0(Y;\mathbf{A}) \sum_{n=0}^{N} \sum_{m=0}^{M} C_{mn}\, \phi_m(Y)\, \psi_n(Z). \tag{14}$$

Here $U_0(Y;\ \mathbf{A})$ is the function that forces the broad Y variation, such as the jet-like character of the flow in (1) while the double summation provides a fine tuning mechanism in Y and Z. It is usual in such an approach to choose the functions $\phi_m(Y)$ and $\psi_n(Z)$ to be orthogonal polynomials, such as Chebyshev or Legendre polynomials.

[75] The fitting process minimized the total weighted least squares error between the data values and the approximation (14). The function $U_0(Y;\ \mathbf{A})$ was chosen to correspond to (1), so that coefficient vector $\mathbf{A}$ is only permitted to contain three components; these are the maximum current magnitude, midpoint and half-width. An initial estimate for each quantity is taken from an initial sweep of the data. The coefficient matrix $\mathbf{C} = \{C_{mn}\}$ initially sets all components to zero, with the exception of C_{00}, which is set to unity. The orthogonal polynomials were chosen to be normalized Legendre polynomials in both the Y and Z directions with typically $N = 5$ and $M = 3$ or 5. The curve fitting method depends critically upon the approximating functions being a good fit to the underlying experimental data and is the main computational effort.

5.1.2. Modeling Considerations

[76] The experimental wave regime was weakly nonlinear with a first harmonic magnitude consistent with linear theory, confirmed by the wave steepness parameter ε ($= ak$) taking the value 0.1 based upon the incident wave conditions. It was also in the deepwater regime, $k_0 h$ taking a value of 3.09. The relative current strength parameter δ ($= U_0/c_0$), denoting the ratio of characteristic current value to the incident phase velocity, has approximate values of 0.15 and 0.16 for the WCO and WCF conditions, respectively, based upon the depth-averaged streamwise centerline velocity values presented in Table 4. Caustics should not occur for the primary wave trains. The deepwater relation (8) predicts caustics for the WCF condition $U_0/c_0 = 0.16$ when $\alpha_0 < 40°$; alternatively, if $\alpha_0 = 60°$, then caustics would not appear unless $U_0/c_0 > 0.32$. Thus the use of the wave ray model is validated on parametric grounds but the importance of the acknowledged vertical shear in the current can only be determined by a comparison of prediction and measurement.

[77] The range of validity of the MCA (section 4.3), can be determined from the relative magnitudes of the wave steepness parameter ε and the relative current strength parameter δ. *Thomas and Klopman* [1997] introduced a classification scheme that defines moderate currents by $\varepsilon \ll \delta \ll 1$ and weak currents by $\delta = O(\varepsilon) \ll 1$. For the values established above, $\varepsilon = 0.1$ and $\delta = 0.16$, the current may be considered weak relative to this criterion. (In the weak current approximation, the magnitude of the change in the first harmonic term is of the same order as the magnitude of the second harmonic in the Stokes wave series.) However, it can be shown that the averaged Lagrangian in (9) and (10) is valid for both moderate and weak currents, so the MCA formulation introduced in section 4.3 remains applicable in the present context.

5.2. Model Comparison

5.2.1. Velocities

[78] Wave velocities were predicted by the two methods described in section 4. In each case the input provided was the local water depth h, the wave frequency ω, a wave amplitude a_0 and the streamwise current profile $\overline{U}(y)$ or $U(y,\ z)$ in the presence of waves. The incident wave amplitude a_0 for both the WCF and WCO conditions was taken to be 0.0154 m.

[79] No x variation was included in the current and no attempt was made to predict the velocities on a wave-by-wave basis. Thus the predictions provide an averaged description, over the duration of the measurements, approximately 750 wave periods, during which the current may exhibit significant variations (see Figure 6). The comparison between prediction and measurement for the magnitude of the first harmonic of the vertical velocity component is shown in Figures 17 and 18 for the WCF and WCO, respectively, at all measuring stations. It should be noted that the maximum current occurs approximately at station G for the following case, whereas for the opposing current it occurs at station D (see Figure 9). Two velocity measures are shown. These are the first harmonic obtained directly from the time series (the ensemble average) and a spectral measure of the first harmonic obtained from the narrow band around the peak spectral frequency. These two quantities were indistinguishable in the wave-alone cases and the difference in the combined tests was attributed to the effect of the temporal variability in the current. At the offshore edge of the current, station A, there is little difference between the two velocity measures, as the surface elevation is relatively stable. As the waves progress across the current, the temporal variation in the surface elevation increases (see Figure 12), with a corresponding increase in difference between the ensemble average and spectral measures.

[80] It is clear from Figures 17 and 18 that there is almost no difference between the MCA prediction and the ray-

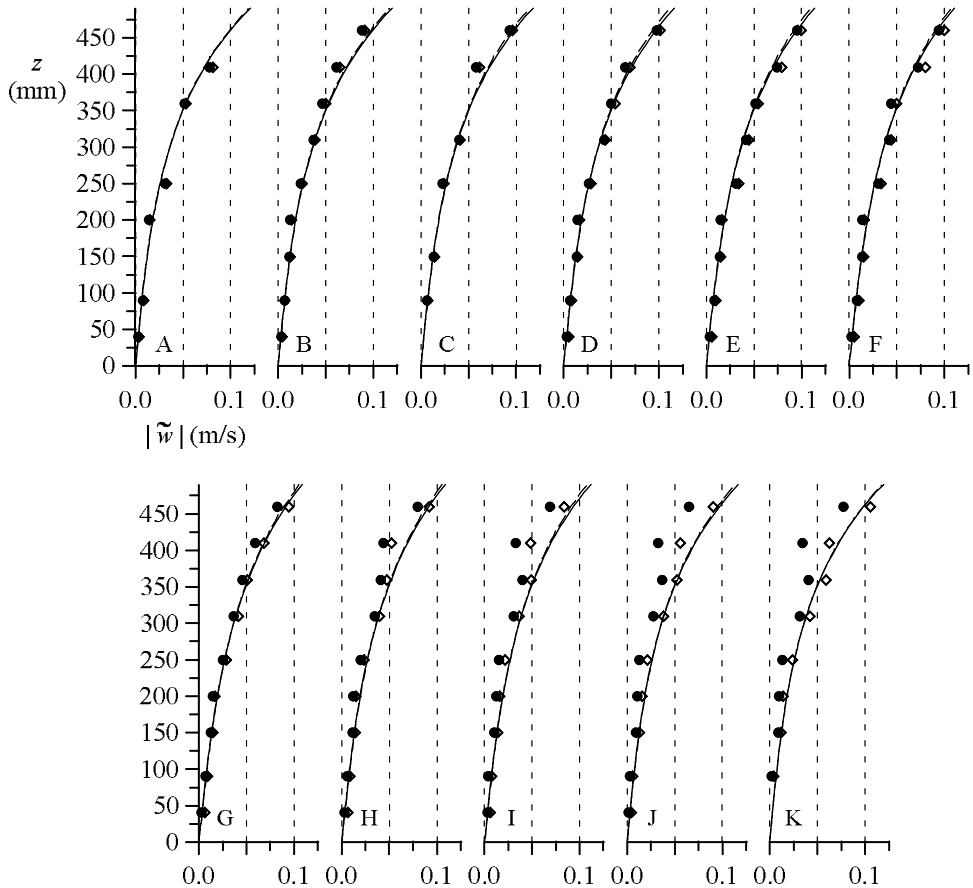

Figure 17. Model prediction for the first harmonic of the vertical velocity component for the WCF condition: MCA model (solid lines), ray-tracing model (dashed lines), ensemble average (circles), and spectral measure (diamonds). Station A is farthest offshore; station K farthest onshore.

tracing model. Very minor differences occur near the free surface, where the influence of the surface shear is likely to be most significant. However, it is known that good working approximations to the wave kinematics can be obtained in two dimensions by employing a depth-averaged current approximation to the mean flow profiles observed in the experiment. As the present models do not permit x variation, they are both essentially quasi-two-dimensional. Thus the present finding is not unexpected, following determination of the current profile.

[81] The comparison between the velocity profiles shows that acceptably good predictions are obtained in both the WCF and WCO conditions. Two general comments can be made. First, the predictions are typically closer to the spectral measure than to the ensemble average. Second, the accuracy of the fit decreases as the waves progress across the current and the surface elevation becomes temporally less stable. The MCA model will predict the correct vertical variation in the wave-like velocity profile for a given input current established from the curve fitting process with its inherent balance of numerical exactness and smoothing. A more precise fit to the current may improve the agreement.

5.2.2. Elevations

[82] Both the ray-tracing and MCA models utilize conservation relations to predict the local amplitude (or wave height), local phase speed, the angle of incidence and the wave number (or wavelength) across the current. These are given in (5)–(7) and (11)–(13) and the required input data correspond to the incident wave conditions together with the varying current profile. It is clear from the agreement between prediction and experiment, particularly with the spectral amplitude measure, that the conservation relations have provided reasonably accurate values of the individual quantities. The applicability of such an approach is contingent upon the absence of wave reflection, as verified in the present experimental study. A consequence is that it is also feasible to attempt to determine these quantities directly from the surface record. For a regular wave of frequency ω propagating through a homogeneous medium, the phase difference $\Delta\ \theta$ between any two locations, with a known spatial separation (Δx, Δy), is a function of the wave phase speed c and the wave propagation direction α. From the definition of the phase function

$$\theta\,(x,y,t) = k\cos\alpha\,x\ +\ k\sin\alpha\,y\ -\ \omega\,t,$$

it is straightforward to show

$$\Delta\theta = \frac{\omega}{c}(\Delta x\cos\alpha + \Delta y\sin\alpha). \tag{15}$$

The derivation assumes that the wave properties are uniform throughout the measuring region which can only be approximate in the current region. Thus experimental estimates of α and c determined in this way correspond to

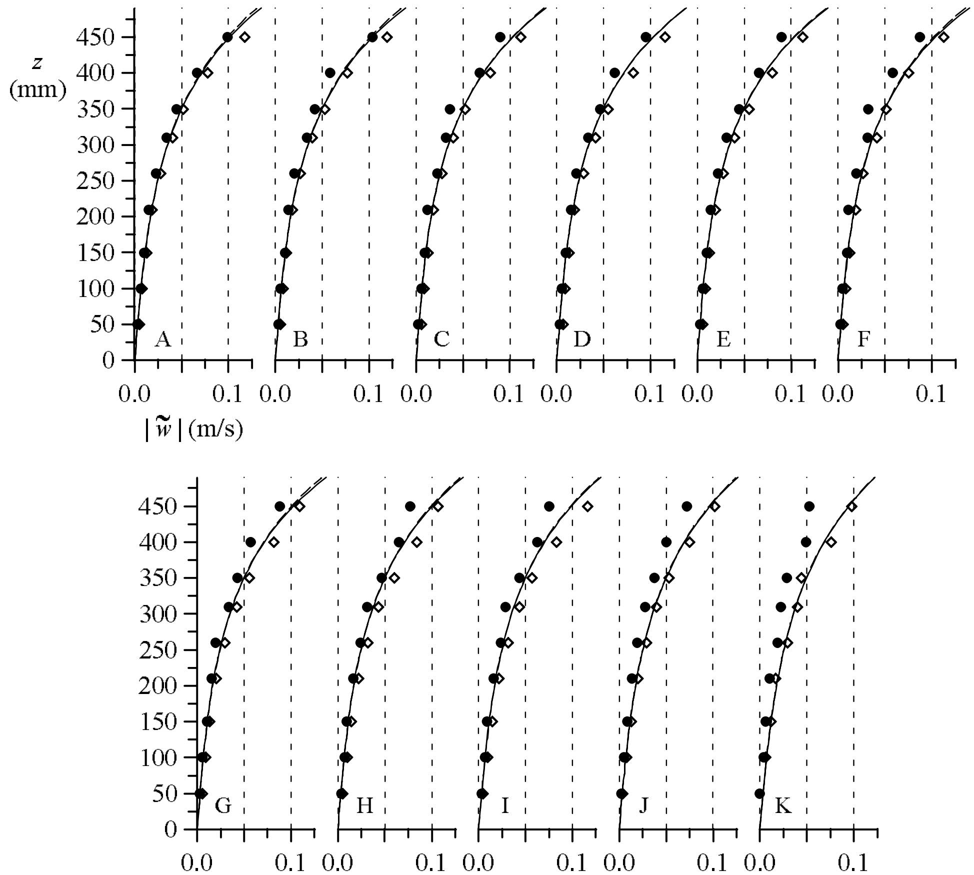

Figure 18. Same as Figure 17 but for the WCO condition.

an averaged value in the region; repeated application will provide a set of averaged values across the current. If a more sophisticated version of (15) were employed to take account of current changes, then this would require an input from the current field and not depend upon surface elevations alone. The wave probe array used in the experiments provided up to seven independent phase differences, including pairs in which x or y is fixed, and a least squares optimization was used to obtain the two unknowns α and c.

[83] The predictions and measurements of c, α and H are shown in Figures 19 and 20 for the WCF and WCO conditions, respectively, together with a schematic showing the position of the data points relative to the current. The wave height data have previously been discussed in section 3.3.2, with particular attention drawn to the behavior in wave height on the shore edge of the current. Such variation is also present in the c and α data, and is more marked for the opposing current than for the following one, as is the case for the wave height. The behavior was attributed to secondary recirculations in the basin and the additional data support this conjecture. However, the additional data suggest that the secondary recirculations must contain a strong shear layer.

[84] As expected the predictions of the conservation relations for the ray-tracing and MCA models are broadly similar in all cases. Such differences that do exist are closely linked to the presence of the shear layer in the mean current. This is of interest, since the differences are more noticeable than those that appear in the corresponding velocity profiles in Figures 17 and 18 and can only be attributable to inclusion of vertical variation in the current profile. Both models predict the phase velocity c reasonably well, although there is a slight underprediction for the following current. The variation in propagation angle is also well predicted in the WCO case. Wave height is reasonably predicted for the WCF case but less so for the WCO condition, in direct contrast to that identified for the phase velocity.

[85] The unexpected feature is the variation of the propagation angle α in the WCF case. If the analysis was valid for a long-crested wave train, then the behavior would be interpreted as corresponding to a twin-jet current, with two independent refraction patterns and this clearly was not the case. The data were obtained by employing three four-probe combinations, which yielded consistent readings, so the cause can only be a physical phenomenon or a result of the numerical solution procedure. As the predicted and measured velocity components agree to a reasonable degree of accuracy, there is unlikely to be a physical cause. A more careful examination of the phase speed in Figure 19 shows that not only does the model appear to underpredict consistently the c data but also that there is a slight dip in the data where a maximum would be expected. There is also more scatter over the center of the current for both c and α in the WCF condition than in the WCO case. The application of the least squares method is straightforward but determines $c \sin \alpha$ and $c \cos \alpha$ simultaneously, with further

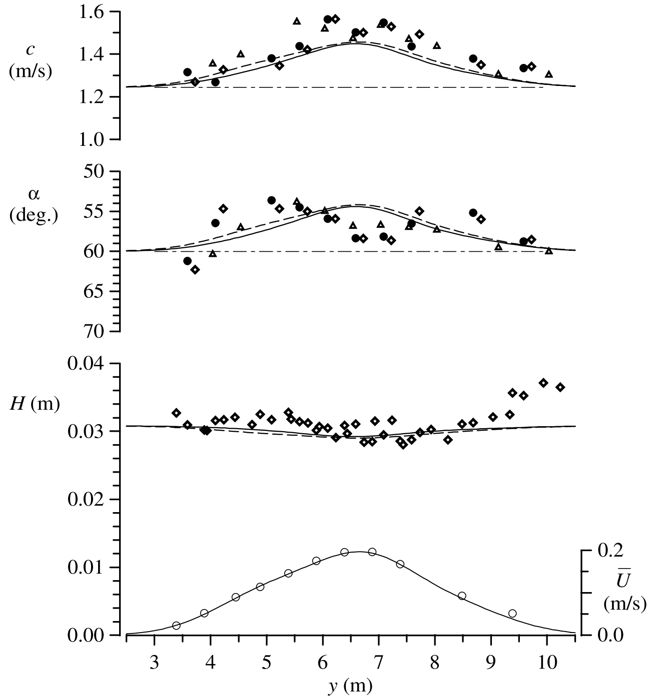

Figure 19. Model predictions of the phase speed, c, propagation angle, α, and wave height, H, for the WCF condition. Symbols are as follows: solid line, MCA model; dashed line, ray-tracing model; circle, streamwise current $\overline{U}$; diamond, solid circle; and triangle, different probe combinations in c and α.

steps then necessary to separate them. It is not surprising that both display similar traits.

6. Discussion

[86] The flow conditions studied here represent a challenging experimental problem, as large-scale flows are inherently turbulent and not unidirectional. Considerable time was devoted to the creation of a stable laterally and vertically sheared shore-parallel jet-like current. The deceleration and lateral spreading characteristics correspond broadly to those of a free plane turbulent jet flow while the secondary circulations observed in the lateral shear layers have been previously observed in jet-like currents [*Dracos et al.*, 1992]. These low-frequency eddy structures are two-dimensional, confined to the horizontal plane. Their presence within the current changes a nominally steady two-dimensional flow into an unsteady three-dimensional one, an effect which is found in natural jet-like currents but one that is not accounted for in the models. Such vortical structures are known to have a significant effect on wave propagation characteristics when their length scale is comparable to, or greater than, a wavelength [*Peregrine*, 1976] and are primarily responsible for the increased temporal variability of the surface elevation shoreward of the current and the broadening of the spectral peaks. The temporal and spatial periodicity of the eddies is supported by the periodic features in the temporal modulation pattern of the surface elevation. A regular distribution of nodes and antinodes moving over the region shoreward of the current was observed during the experiment.

[87] Substantial changes to the mean current field, in both vertical and horizontal profiles, were observed with the addition of waves. Little change was expected for normal incidence, as laminar/inviscid theory predicts changes in ray path but no dynamic interaction, however the resulting vertical profile at the centerline exhibited an almost straight line variation. In the following and opposing wave cases, the change in the vertical profiles from those observed in the current alone case were not strictly comparable with the changes in the mean flow that are known to be experienced in two-dimensional wave-current interaction [see *Groeneweg and Klopman*, 1998]. While the following wave case displayed a characteristic reduction in flow rate in the upper part of the water column, the characteristic increase associated with the opposing wave case was not apparent. The opposing wave case actually displayed a reduced flow rate over the whole water column. This is consistent with the observations of *Ismail and Wiegel* [1983] for a collinear wave and jet current which displayed a reduced mean depth-averaged centerline velocity and an increased current half-width. The lateral displacement of the mean current, in particular the offshore shift for the opposing wave case, is an interesting feature of three-dimensional wave-current interaction. While the mechanisms identified in existing two-dimensional theories [e.g., *Groeneweg and Klopman*, 1998] may offer an explanation of the present observations, the extension of this theory to three dimensions remains an outstanding and important area of research.

[88] For the wave-current regime of the experiments, the ray-tracing model, based on linear irrotational theory and a depth-averaged current, worked extremely well over the majority of the current. This provides considerable confi-

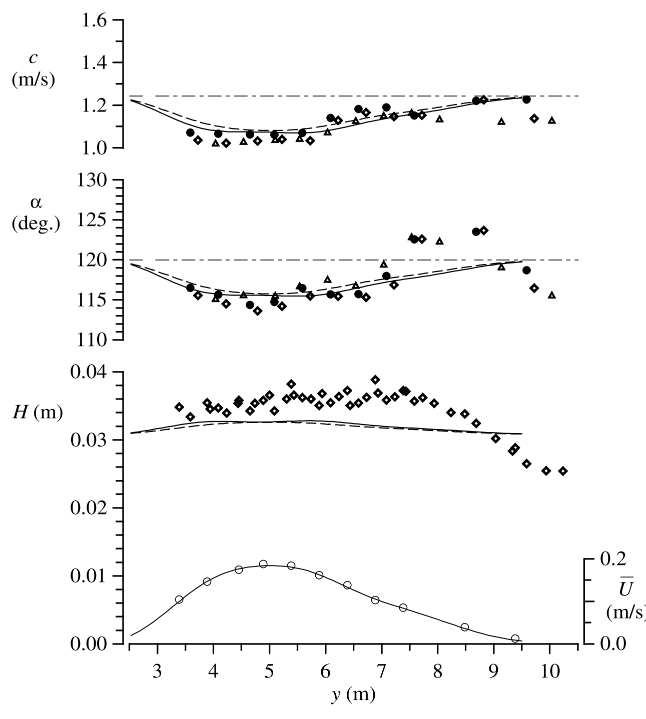

Figure 20. Same as Figure 19 but for the WCO condition.

dence in the use of such methods in practical applications. The poorer agreement observed shoreward of the current maximum coincides with an increasingly modulated wave field produced by the secondary circulations within the current and nonuniformity in the streamwise direction. In this region the assumption of a quasi two-dimensional flow field is strictly no longer valid. However, such features are undeniably present in the field and need to be accounted for in full-scale modeling.

[89] The more sophisticated models showed no significant improvement in prediction. As stated earlier, the Mild Shear model did not predict reflection and consequently its predictions reduced to those of the ray-tracing model. The experimental parameter values (U_0/c_0, k_0b) were (0.16,11.9) and (0.15,13.0) for the WCF and WCO conditions respectively. The nondimensional length scale of the spanwise current variation used here, k_0b, is equivalent to the parameter $\beta = \omega^2 L_c/g$ proposed by *McKee* [1987]. For reflections to be appreciable at the angles of incidence considered here, the Mild Shear model would require the value of k_0b to be an order of magnitude smaller. This is consistent with earlier two-dimensional studies suggesting that shear on the length scale of a wavelength, $k_0b = O(2\pi)$, is sufficient for slowly varying conditions and that no appreciable reflection is expected unless k_0b is considerably smaller than this [*Thomas*, 1981].

[90] Although the current possessed vertical variation, it is known from two-dimensional applications that the velocity field can be well predicted by depth-averaged models for such profiles. While it is unclear how vertical variation in the current profile can be incorporated into models adopting the Mild Shear approach, the moderate current approximation provides a mechanism for accounting for the effect of vertical shear.

7. Conclusions

[91] A unique and challenging experiment to investigate the transformation of gravity waves by a narrow jet-like current possessing both horizontal and vertical shear has been performed, producing detailed velocity and surface elevation measurements of the flow field. Negligible reflection from the horizontal shear layers of the current was observed. The refraction of waves obliquely incident to the current was significant: waves becoming increasingly current parallel as a following current strength increased, and becoming increasingly current normal on an opposing current. On the current, measured wave height decreased in the following case and increased in the opposing case. These trends are predicted well by the simple wave ray model of wave transformation on a constant-over-depth slowly varying current. A more sophisticated moderate current approximation model, incorporating the effect vertical shear, showed no significant improvement in prediction for the present experimental conditions. However, the moderate current approximation provides the first step toward accounting for the effect of vertical shear typically found in many jet-like currents encountered in the nearshore, coastal and ocean regions.

[92] **Acknowledgments.** The experimental data were obtained as part of the project The Kinematics and Dynamics of Wave-Current Interactions, which was funded by the Commission of the European Communities, Directorate General for Science, Research and Development, under contract MAS3-CT95-0011 of the MAST programme.

References

Dalrymple, R. A. (1973), Water wave models and wave forces with shear currents, *Tech. Rep. 20*, Coastal and Ocean Eng. Lab., Univ. of Fla., Gainesville.

Dracos, T., M. Giger, and G. H. Jirka (1992), Plane turbulent jets in a bounded fluid layer, *J. Fluid Mech.*, *241*, 587–614.

Evans, D. V. (1975), The transmission of deep-water waves across a vortex sheet, *J. Fluid Mech.*, *68*, 389–401.

Groeneweg, J., and G. Klopman (1998), Changes of mean velocity profiles in the combined wave-current motion described in a GLM formulation, *J. Fluid Mech.*, *111*, 15–25.

Hales, L. Z., and J. B. Herbich (1972), Tidal inlet current—Ocean wave interaction, in *Proceedings of 13th International Conference on Coastal Engineering, Vancouver, Canada*, pp. 669–688, Am. Soc. of Civ. Eng., Reston, Va.

Hamm, L., P. A. Madsen, and D. H. Peregrine (1993), Wave transformation in the nearshore zone: A review, *Coastal Eng.*, *21*, 5–39.

Hughes, B. A., and R. W. Stewart (1961), Interaction between gravity waves and a shear flow, *J. Fluid Mech.*, *10*, 385–400.

Isaacson, M. (1991), Measurement of regular wave reflection, *J. Waterw. Port Coastal Ocean Eng.*, *117*, 553–569.

Ismail, N. M. (1984), Wave-current models for design of marine structures, *J. Waterw. Port Coastal Ocean Eng.*, *110*, 432–447.

Ismail, N. M., and R. L. Wiegel (1983), Opposing wave effect on momentum jets spreading rate, *J. Waterw. Port Coastal Ocean Eng.*, *109*, 465–483.

Jonsson, I. G. (1990), Wave current interactions, in *The Sea*, *Ocean Eng. Sci.*, vol. 9A, edited by B. Le Méhauté and D. M. Hanes, pp. 65–120, Wiley-Interscience, Hoboken, N. J.

Jonsson, I. G., O. Brink-Kjaer, and G. P. Thomas (1978), Wave action and set-down for waves on a shear current, *J. Fluid Mech.*, *87*, 401–416.

Kemp, P. H., and R. R. Simons (1982), The interaction between waves and a turbulent current: Waves propagating with the current, *J. Fluid Mech.*, *116*, 227–250.

Kemp, P. H., and R. R. Simons (1983), The interaction between waves and a turbulent current: Waves propagating against the current, *J. Fluid Mech.*, *130*, 73–89.

Kirby, J. T. (1984), A note on linear surface wave-current interaction over slowly varying topography, *J. Geophys. Res.*, *89*, 745–747.

Kirby, J. T. (1986), Comments on 'The effects of a jet-like current on gravity waves in shallow water,' *J. Phys. Oceanogr.*, *16*, 395–397.

Klopman, G. (1994), Vertical structure of the flow due to waves and current, *Prog. Rep. H840.30, Part 2*, Delft Hydraul., Delft, Netherlands.

Lake, B. M., H. C. Yuen, H. Rungaldier, and W. E. Ferguson (1977), Nonlinear deep-water waves: Theory and experiment. part 2. Evolution of a continuous wave train, *J. Fluid Mech.*, *83*, 49–74.

Lavrenov, I. V. (2003), *Wind-Waves in Oceans: Dynamics and Numerical Simulations*, Springer, New York.

Longuet-Higgins, M. S., and R. W. Stewart (1961), The changes in amplitude of short gravity waves on steady non-uniform currents, *J. Fluid Mech.*, *10*, 529–549.

Longuet-Higgins, M. S., and R. W. Stewart (1964), Radiation stresses in water waves: A physical discussion with applications, *Deep Sea Res. Oceanogr. Abstr.*, *11*, 529–562.

MacIver, R. D. (2001), The transformation of gravity waves by a horizontally sheared current, Ph.D. thesis, Univ. College London, London, U. K.

MacIver, R. D., R. R. Simons, and G. P. Thomas (2001), A comparison of experimental measurements and theoretical predictions for three-dimensional wave-current interactions, in *Proceedings of Coastal Dynamics '01, Lund, Sweden*, pp. 142–151, Am. Soc. of Civ. Eng., Reston, Va.

McKee, W. D. (1977), The reflection of water waves by shear currents, *Pure Appl. Geophys.*, *115*, 937–949.

McKee, W. D. (1987), Water wave propagation across a shearing current, *Wave Motion*, *9*, 209–215.

McKee, W. D. (1996), A model for surface wave propagation across a shearing current, *J. Phys. Oceanogr.*, *26*, 276–278.

Mei, C. C., and E. Lo (1984), The effects of a jet-like current on gravity waves in shallow water, *J. Phys. Oceanogr.*, *14*, 471–477.

Peregrine, D. H. (1976), Interaction of water-waves and currents, *Adv. Appl. Mech.*, *16*, 9–117.

Sand, S. E., and A. E. Mynett (1987), Directional wave generation and analysis, in *Proceedings of IAHR Seminar, Wave Analysis and Generation in Laboratory Basins, XXII Congress, Lausanne, Switzerland*, pp. 209–235, Int. Assoc. for Hydraul. Res., Madrid.

Simons, R. R., and R. D. MacIver (2000), Experimental determination of wave lengths in the presence of a mean current, *Coastal Eng.*, *41*, 413–431.

Simons, R. R., R. J. S. Whitehouse, R. D. MacIver, J. Pearson, P. B. Sayers, Y. Zhao, and A. R. Channell (1995), Evaluation of the UK Coastal Research Facility, in *Proceedings of Coastal Dynamics '95, Gdansk, Poland*, pp. 161–172, Am. Soc. of Civ. Eng., Reston, Va.

Skop, R. A. (1987), An approach to the analysis of the interaction of surface waves with depth-varying current fields, *Appl. Math. Model.*, *11*, 432–437.

Smith, J. R. (1983), On surface gravity waves crossing weak current jets, *J. Fluid Mech.*, *134*, 277–299.

Taylor, G. I. (1938), The spectrum of turbulence, *Proc. R. Soc. London, Ser. A*, *164*, 476–490.

Tennekes, H., and J. L. Lumley (1972), *A First Course in Turbulence*, MIT Press, Cambridge, Mass.

Thomas, G. P. (1981), Wave-current interactions: An experimental and numerical study. part 1. Linear waves, *J. Fluid Mech.*, *110*, 457–474.

Thomas, G. P. (1999), Reflection analysis for small waves in two and three dimensions, in *The Kinematics and Dynamics of Wave-Current Interactions*, final report, contract MAS3-CT95-0011, pp. 1–21, Eur. Union Mar. Sci. Technol. Programme, Brussels, Belgium.

Thomas, G. P., and G. Klopman (1997), Wave-current interactions in the near-shore region, in *Gravity Waves in Water of Finite Depth*, *Adv. Fluid. Mech.*, vol. 10, edited by J. N. Hunt, pp. 255–319, Comput. Mech., Billerica, Mass.

White, B. S. (1999), Wave action on currents with vorticity, *J. Fluid Mech.*, *386*, 329–344.

R. D. MacIver and R. R. Simons, Department of Civil and Environmental Engineering, University College London, London, WC1E 6BT, UK. (r.maciver@ucl.ac.uk)

G. P. Thomas, Department of Applied Mathematics, University College Cork, Cork, Ireland.